

Integrating behavioral experimental findings into dynamical models to inform social change interventions

Radu Tanase,¹ René Algesheimer,¹ and Manuel S. Mariani¹

URPP Social Networks, University of Zurich, CH-8050 Zurich, Switzerland

Addressing global challenges – from public health to climate change – often involves stimulating the large-scale adoption of new products or behaviors. Research traditions that focus on individual decision making suggest that achieving this objective requires better identifying the drivers of individual adoption choices. On the other hand, computational approaches rooted in complexity science focus on maximizing the propagation of a given product or behavior throughout social networks of interconnected adopters. The integration of these two perspectives – although advocated by several research communities – has remained elusive so far. Here we show how achieving this integration could inform seeding policies to facilitate the large-scale adoption of a given behavior or product. Drawing on complex contagion and discrete choice theories, we propose a method to estimate individual-level thresholds to adoption, and validate its predictive power in two choice experiments. By integrating the estimated thresholds into computational simulations, we show that state-of-the-art seeding methods for social influence maximization might be suboptimal if they neglect individual-level behavioral drivers, which can be corrected through the proposed experimental method.

Preventing, mitigating, and solving some of the most pressing challenges faced by mankind often requires the design of effective technological and behavioral solutions. But even the most effective solutions would fail to make an impact without their large-scale adoption by the world population. For some global challenges, such as the COVID-19 pandemic, policymakers around the world have often enforced the required behaviors to counteract the pandemic’s most severe effects in a top-down fashion, e.g., by restricting travel, requiring mandatory mask-wearing in public spaces, and isolating positive cases. For other global challenges, even when technological and behavioral solutions to mitigate the challenge are available, policymakers are unwilling to or cannot fully oblige the citizens to adopt them [1]. This is the case, for example, for shifting individuals’ transportation, nutrition, and building design choices toward sustainable alternatives, which might substantially reduce greenhouse gas emissions [2]. Many sustainable technologies and behaviors are well-known, but triggering their large-scale adoption remains elusive [1].

To generate scientific insights that could inform societal change policies, a tension between two approaches exists. A well-established research tradition – e.g., in microeconomics, consumer behavior, and psychology – focuses on modeling the individual-level decision-making process, seeking to capture the drivers of individual-level choices and potentially nudge new behaviors [3–6]. These approaches typically capture the complexity of individual decision-making processes, which leads in the best case to a precise image of individual processes. However, because of the feedback mechanisms and consequent nonlinearities that characterize collective behaviors, their conclusions may not be directly extrapolated to the collective level [7–13].

On the other hand, computational approaches to understanding collective behavior in complex systems typically formulate parsimonious models on individual-level behaviors under simplifying assumptions. These ap-

proaches – often rooted in statistical physics and agent-based modeling – have found applications ranging from materials composed of simple particles to systems composed of more sophisticated units such as flocks [14], swarms [15], crowds [10], and societies [11]. In the context of social change, computational approaches leverage agent-based simulations to determine the system-level implications of interconnected individual-level choices [7–13, 16]. These models enable a comprehensive understanding of the possible macro-level behaviors of a system, but when not calibrated with empirical individual processes, they may fail to identify the best intervention for a given scenario [17]. Individual-level and computational approaches are mainly developed in parallel. Scholars from various disciplines have argued that the disconnect between our understanding of individual decision-making and social network dynamics limits policymakers’ ability to stimulate effective collective behavioral responses to increasingly complex global challenges [18], and called for data-driven efforts to integrate the two perspectives [13, 18–21]. Here, we demonstrate how the two approaches can be integrated in the context of new product or behavior adoption, and how such an integration can inform network interventions for social change.

The leading framework to model social change is provided by the complex contagion theory [7, 8, 22–25]. Complex contagion describes accurately how new ideas and behaviors spread in many policy-relevant contexts, including the adoption of healthy behaviors [26–29], online social platforms [30–32], new technologies [33, 34], views on political and controversial topics [35–38], social movements and political protests [7, 39, 40], the abandonment of harmful cultural traditions [16] – see Guilbeault et al. [23] for a comprehensive review. Complex contagion models link individual-level and collective dynamics by assuming that choices are determined by an individual-level behavioral trait – her threshold level. Yet surprisingly, there is little evidence on the empirical individual-level threshold levels [19, 41], and a scarcity of

studies attempting to link empirical thresholds with the collective dynamics of new product and behavior adoption processes.

Here we demonstrate that individual-level threshold levels can be derived from individual-level choice models traditionally used in microeconomics, social psychology, and consumer behavior. We leverage a simple formula that links individuals' thresholds to the drivers of individual-level adoption choices, which enables the measurement of individual-level thresholds from discrete-choice experiments. Results from two choice experiments demonstrate that individual-level thresholds can be estimated from choice data and used to make accurate out-of-sample choice predictions at the individual level. We show how the estimated thresholds can be integrated into policies to promote large-scale behavioral change. To this end, we compare the performance of policies aware of the estimated thresholds against traditional ones based on social network centrality, and we determine under which conditions the threshold-aware policies outperform existing ones. For example, our findings reveal that the recently-introduced complex centrality [41] can only outperform state-of-the-art policies when its calculation takes into account the estimated thresholds. We conclude by showing how the proposed framework might benefit a broader class of social spreading models, including innovation diffusion [42] and preferential attachment models [43].

RESULTS

From individual-level preferences to complex contagion

The core insight from the complex contagion theory is that when an adoption choice involves a substantial level of personal investment (e.g., effort, monetary cost, personal or reputational risk), it requires a sufficient level of social reinforcement from the decision-maker's social contacts who already adopted the new product or behavior [1, 22–24]. This idea is incorporated in the threshold model of new product diffusion [8, 22], where individual n adopts a given product (or behavior) i if and only if at least a threshold fraction τ_{ni} of her social contacts already adopted the product. The relevance of the threshold distribution for diffusion outcomes [7, 8] seems to directly call for efforts to measure individual-level thresholds from empirical data to calibrate threshold-based simulations.

However, progress in this direction is lacking [19, 23, 41]. Seemingly insurmountable challenges occur when we seek to measure a given individual's threshold for a given product from historical adoption data. If a given individual never adopted the product, we do not know at which higher level of social signal, if any, she would have adopted it. Or conversely, if she already adopted, for which lower level of social signal she would have still adopted. Besides, if the product is new, historical adop-

tion data does not exist. To bypass these challenges, we draw inspiration from the consumer behaviour techniques routinely used to estimate consumers' willingness-to-pay for a given product [3, 44, 45], and we reinterpret individual-level thresholds to adoption in terms of a discrete-choice problem [3]. In doing so, we connect the complex contagion literature with the individual-level perspective (see Fig. 1A).

We assume that when evaluating a certain product (or behavior) i , an individual is influenced by both the product's attributes and the received social signal about the product. We assume that individual n 's utility from adopting product (or behavior) i consists of two terms: the utility of the product attributes for n ($U_{ni}^{(A)}$) and the "social utility" [46] derived from the social signal received by n about i ($U_{ni}^{(S)}$): $U_{ni} = U_{ni}^{(A)} + U_{ni}^{(S)}$. Under this formulation, we define the adoption threshold as the minimal level of the social signal for which the utility of n from adopting i exceeds n 's status-quo utility, i.e., the utility from not adopting ($U_n^{(0)}$, see Fig. 1B). In the following, it is convenient to define n 's resistance to adopting i as the gap between her status-quo utility and the attribute utility from adopting i , i.e., $R_{ni} = U_n^{(0)} - U_{ni}^{(A)}$. Assuming that $R_{ni} > 0$ and the social utility is linear in the number of adopters ($U_{ni}^{(S)} = \gamma_n s_{ni}$, where s_{ni} denotes the percentage of adopters of i within n 's social neighborhood, and γ_n represents n 's marginal utility of the social signal), the adoption threshold can be expressed as [47]:

$$\tau_{ni} = \frac{U_n^{(0)} - U_{ni}^{(A)}}{\gamma_n} = \frac{R_{ni}}{\gamma_n}. \quad (1)$$

This result is intuitive: The higher the individual's resistance, or the lower the weight of the social signals on her choices, the higher her threshold. We assume – as typical in discrete choice modeling [3] – that the attribute utility is linear in the attributes: $U_{ni}^{(A)} = \sum_{k=1}^K \beta_{nk} x_{ki}$, where x_{ki} encodes the extent to which alternative i exhibits attribute k and β_{nk} is referred to as the partworth utility of n for attribute k .

An implication of Eq. (1) is that, if one is able to estimate individuals' R and γ from choice data, one can directly calculate her threshold as well. Before providing the results of this procedure, we anticipate that, given estimates \hat{R}_{ni} and $\hat{\gamma}_n$ of individual resistance and marginal utility from social signal, Eq. (1) can lead to multiple scenarios. We refer to individuals with $0 < \hat{R}_{ni} < \hat{\gamma}_n$ as *susceptible* adopters: For these individuals, Eq. (1) delivers $\hat{\tau}_{ni} \in (0, 1)$, which implies that their adoption choices for product i are influenced by different levels of social signals $s_{ni} \in (0, 1)$. For individuals with $\hat{R}_{ni} < 0$, Eq. 1 delivers $\hat{\tau}_{ni} < 0$; these individuals correspond to the innovators in Rogers' innovation diffusion theory [48], as they adopt as soon as they become aware of product i regardless of the social signal's strength; for practical purposes, their estimated threshold can be set to zero. For individuals with $\hat{R}_{ni} > \hat{\gamma}_n$, Eq. 1 delivers $\hat{\tau}_{ni} > 1$; these individuals will never adopt product i regardless of the social

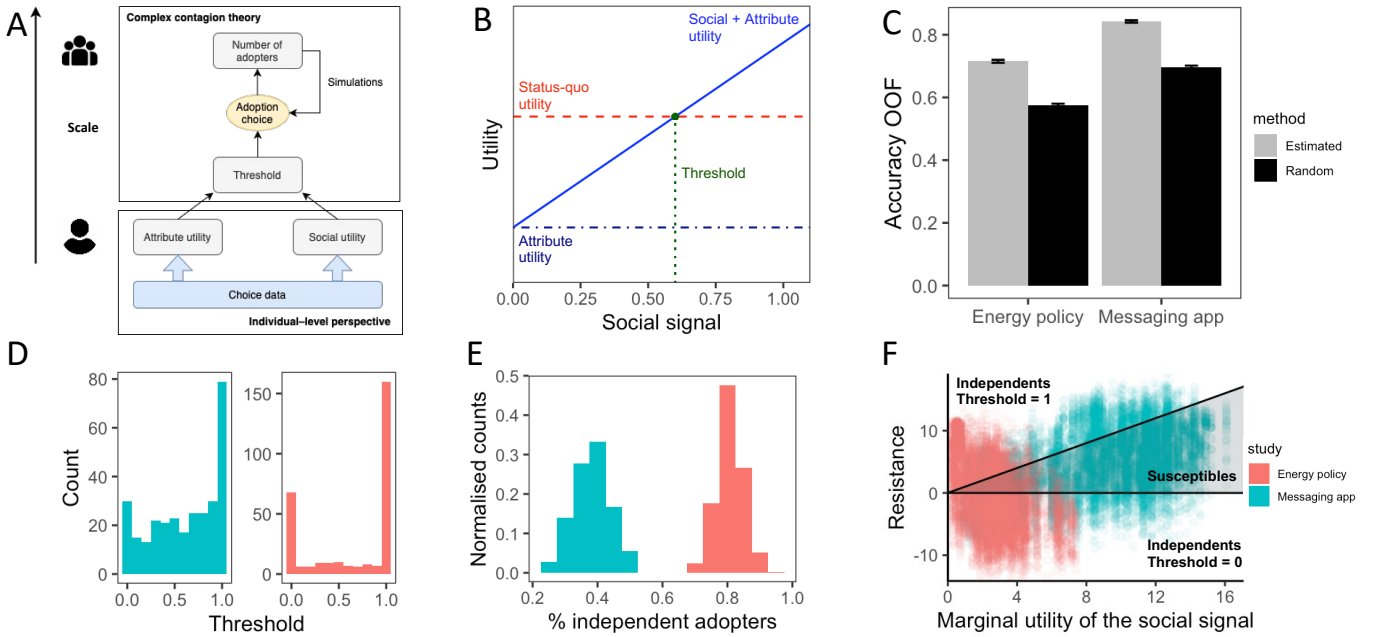


Fig. 1: **Estimating individual-level thresholds.** (A) The complex contagion theory assumes that individual-level adoption choices are determined by the decision-makers’ threshold. On the other hand, individual-level perspectives focus on estimating individuals’ utilities of adopting from choice data. Our work reconciles the two perspectives by reinterpreting the individual-level thresholds in terms of individuals’ attribute and social utilities. (B) For a susceptible adopter, the status-quo utility is initially larger than the utility from adopting. As the number of adopters increases, so does her social utility. The threshold is defined as the minimal level of social signal at which the utility from adopting exceeds the utility from not adopting. (C) For both experiments, the individual-level thresholds estimated from experimental data hold out-of-sample predictive power, as illustrated by their superior accuracy compared to a random-threshold baseline. (D) In general, different products exhibit different threshold distributions, as illustrated by the two examples provided here (instant messaging app in blue; energy policy in orange). (E) The distribution of the proportion of independent adopters (as opposed to susceptible adopters) is significantly lower for the app adoption experiment (AA, in blue) than for the policy support experiment (PS, in orange), which highlights the importance of context for the distribution of individual thresholds. (F) An individual is susceptible for adopting a given product when her resistance is positive and lower than the marginal utility of social signal, which corresponds to the gray stripe in the $\gamma - R$ diagram. There are significantly more observations that fall within the gray stripe in the AA experiment than in the PS experiment, which explains the higher percentage of susceptible adopters in the AA experiment. Data in this panel is based on a sample of products, as described in Supplementary Note S2 B.

signal’s strength; for practical purposes, their estimated threshold can be set to one. We refer to individuals with $\hat{R}_{ni} < 0$ or $\hat{R}_{ni} > \hat{\gamma}_n$ as *independent* adopters, as their adoption choices are independent of the level of social signal.

This interpretation of the threshold has two important implications. First, we can unlock the connection between individual-level utilities and threshold-based diffusion processes, thereby connecting macro-level patterns of adoption with their micro-level drivers (see Figs. 1A–B). Second, given empirical choice data, we can estimate the individual-level thresholds from choice data through well-established utility estimation algorithms [49], which we demonstrate next.

Experimental validation

To demonstrate the detectability of individual-level thresholds from choice data, we rely on choice-based conjoint experiments [50] (see Supplementary Note S1 A for an overview). In this class of experiments, widespread in consumer behavior research, participants are exposed to a set of choices among hypothetical products (represented by combinations of attributes) and a status quo option (selecting none of the presented choices). In the designed experiments, detailed below, participants are exposed to product alternatives characterized additionally by varying levels of social signal. By analyzing the resulting choice data through a well-established Hierarchical Bayes (HB) algorithm [49], we recover the relative weight of each attribute in determining each participant’s

choices (i.e., the parameters β above), the marginal utility the social signal (γ), and the status quo utility ($U^{(0)}$), which enables the calculation of individual thresholds through Eq. (1) (see Methods for the details).

We run two choice-based conjoint experiments, which cover two choice contexts where the complex contagion theory is expected to apply [23]: political views (energy policy support experiment, hereafter PS experiment), and the adoption of a new technology under network externalities (instant messaging app adoption, hereafter AA experiment). In the PS experiment, participants are presented with a set of energy policies regarding carbon-capturing technologies, and in each choice task, they are asked to select which policy they would support (if any). The policies differ in terms of 5 attributes (policy instrument; costs; beginning of policy implementation; required distance to residential areas; policy endorsers) [51] and in their level of social signal (presented as the percentage of peers supporting the policy). The policies' attributes – except for the social signal – are identical to those in ref. [51]. In the AA experiment, participants are presented with a set of messaging apps and are asked to select which app they would consider installing (if any). The apps differ in terms of 4 attributes (accessibility; authentication method; customization level; support for video calls) and their level of social signal (percentage of friends already using the app). For both experiments, we collect choice data from Prolific participants ($N_R = 296$ in the PS experiment and $N_R = 300$ in the AA experiment), and we estimate the individual-level thresholds through the HB algorithm and Eq. (1) (see Methods and Supplementary Note S1 for details about the two studies and the parameter estimation).

Before attempting to understand the properties of the estimated thresholds, it is essential to validate the estimation method. If the estimated thresholds are accurate, we expect that they hold out-of-sample predictive power for individual choices in hold-out tasks that have not been used for the estimation. In particular, for an accurate set of estimated thresholds, we expect that the alternatives selected by the participants in hold-out tasks are predicted by the gap between the alternative's social signal and the individual's threshold for that alternative (see Methods). By translating this remark into an accuracy function (see Eq. (4) in Methods), we can compare the accuracy of choice predictions based on the estimated thresholds against those based on randomly-extracted thresholds from a uniform distribution.

We find that for both the PS and AA experiments, the accuracy of the estimated thresholds on hold-out tasks is significantly larger than that of randomly-extracted thresholds (Fig. 1C). This result indicates that despite the parsimonious assumptions needed to obtain the simple expression in Eq. (1), the estimated thresholds hold significant out-of-sample predictive power, which points to their ability to predict individual choices and motivates a detailed analysis of their properties. Future studies could use the proposed framework to develop and val-

idate more sophisticated threshold estimation methods.

Detection of independent and susceptible individuals

The debate around the shape of the threshold distribution has long stagnated, partly because of the inaccessibility of individual thresholds. The estimated threshold can, therefore, shed light on both the distribution of individual thresholds and its implications for social influence maximization policies. Visual inspections of the threshold distributions for different products reveal that the threshold distribution is strongly product-dependent (see Fig. 1D), which is often neglected in simulation-based studies of social influence maximization. For example, in Fig. 1D, the illustrative energy policy exhibits a strongly polarized, bimodal distribution, with most participants being either supportive of the policy (peak at 0) or unsupportive (peak at 1), regardless of the social signal. By contrast, the instant messaging app represented in the same panel shows a more uniform threshold distribution, with a sizeable number of individuals lying in $(0, 1)$ and, therefore, susceptible to different levels of social signal.

Moving from these case studies to the general properties of the threshold distributions across the two contexts, we quantify the proportion of independent adopters in the two experiments, i.e., the proportion of estimated thresholds equal to zero or one, which denotes a lack of susceptibility to social influence. We find that the proportion of independent adopters is significantly larger in the PS experiment than in the AA experiment (Fig. 1E). This result can be explained in terms of the estimated parameters (Fig. 1F). Assuming the social utility is positive, an adopter is susceptible if and only if $0 < \hat{R}_{ni} < \hat{\gamma}_n$. This condition corresponds to a well-defined “susceptibility stripe” in the two-dimensional $\gamma - R$ diagram (gray area in Fig. 1F) where each individual-product pair is represented by a dot in the plane spanned by the marginal utility of social signal and the resistance. Outside of the susceptibility stripe, the adopter's choice for the product is independent of the social signal. Significantly more individual-product pairs lie within the susceptibility stripe in the AA experiment than in the PS experiment (gray area in Fig. 1F), which explains the lower proportion of independent adopters in the AA experiment (Fig. 1E).

In sum, the estimated thresholds reveal that in different choice contexts, the number of individuals who choose independently of social signals may differ substantially, which is often neglected in extant social influence maximization studies. The high proportion of independent adopters in the PS experiments qualitatively agrees with previous research [52] that found that social norm messages communicating the policies' support level may be ineffective to stimulate carbon-capturing policy support. The two analyzed contexts suggest that the number of independent adopters is smaller in contexts where network externalities influence the adoption more strongly, which

is a conjecture that could be fully validated by future studies.

Implications for seeding policies

Do the estimated thresholds challenge what we know about the maximization of complex contagions? Discrepancies between the threshold distributions observed here and commonly assumed ones (e.g., homogeneous, uniform, and truncated normal distributions) would be irrelevant if the individual threshold values did not matter for social change interventions. This is an implicit assumption, for example, in influence maximization policies based on network centrality. By contrast, we demonstrate here the strong implications of the experimental threshold estimation for social influence maximization.

We consider the seeding problem where a social change practitioner [1] (e.g., a government or an organization) seeks to determine which nodes in a social network to incentivize first to promote the large-scale adoption of a new product or behavior (hereafter, product) [53–56]. To this end, the literature has generated two perspectives. Traditional, *structure-based seeding policies* [53–56] are agnostic to a potential target’s behavioral characteristics, and they select the seeds according to their centrality in the relevant social network. On the other hand, *behavior-based policies* (i.e., policies that take into account individual behavioral characteristics such as the individual thresholds) assume that some individuals are more amenable to change and, therefore, willing to initiate the adoption process for a new product or behavior [16, 57]. The recently-introduced complex centrality [41] constitutes a hybrid policy, as it takes into account both network structure and individual thresholds, but the input thresholds for its calculation are either assumed to be known or extracted from arbitrary distributions, which can lead to suboptimal decisions as shown below. In sum, the estimated thresholds allow us to address the open questions: Under which theoretical conditions can behavior-based (or hybrid) policies outperform structure-based ones?

To address this question, we rely on agent-based spreading simulations based on the threshold model of new product diffusion [8]. In the simulations, $N = 300$ agents are assigned at random to the nodes in the analyzed networks. We analyze the largest components of a subset of the Add Health networks considered by Guilbeault and Centola [41], which include several independent communities that exhibit high variation in network topological properties (see Supplementary Note S2A). We study the independent diffusion of the 36 products analyzed in the AA experiment and a sample of 36 products from those analyzed in the PS experiment (see Supplementary Note S2B for the sampling details). For each product, we assume that the agents make adoption choices based on their *ground-truth thresholds*, which we set to be equal to those estimated from the survey’s par-

ticipants (see Methods). While the ground-truth thresholds used for agents’ adoption decisions are known to the agents, they are not known to the social change practitioner. We assume that the practitioner has been able to survey the nodes of the network with a choice-based conjoint survey and use the collected choice data to estimate the individual thresholds. For our theoretical analysis, as detailed in Supplementary Note S3, we simulate the agents’ answers to the survey based on the parameters estimated from the two experiments, and we use the generated choice data to estimate the individual thresholds (*estimated thresholds*, hereafter) with the same method used for the experimental data (see Methods and Supplementary Note S3). Later, we discuss the robustness of the results in scenarios where only a fraction of the agents can be surveyed.

Under these assumptions, the optimal seeds of behavior-based policies are determined based on the agents’ estimated thresholds. Motivated by the effectiveness of clustered seeding for complex contagions [41, 58], for each policy, we adopt a clustered seeding protocol where we target one focal seed selected by the metric and a subset of her closest neighbors such that $z\% = 2.5\%$ of the nodes are initially active (see Methods) – we show in Supplementary Note S5B that our conclusions are mostly robust with respect to other small values of z . The threshold estimation enables the design of various behavior-based policies: low-threshold policy (where the focal seed is the lowest threshold node); high neighborhood susceptibility policy (where the focal seed is the node with the largest number of low-threshold neighbors); high calibrated complex centrality policy (where the focal seed is the node with the largest complex centrality [41] calculated using the estimated thresholds as inputs). We use various structure-based policies as baselines, which we label according to the metric used to select the focal seed: degree [59], collective influence [54], betweenness [60], closeness [61], and uncalibrated complex centrality (i.e., the nodes’ average complex centrality score over an ensemble of homogeneous threshold values [41] not estimated from actual choice data, see Supplementary Note S4). We also consider a policy where the focal node is selected at random [16]. We refer to Supplementary Note S4 for all the details on the implementation of both the network-based and behavior-based policies.

We evaluate the policies’ performance based on the final number of adopters discounted for the intervention’s cost, i.e., the ratio between the total number of adopters and the cost required for successfully initiating the diffusion (see Methods for the definitions). The performance of each policy depends on the system’s configuration, which is identified by the network being analyzed, the product that spreads through the network, and of the agents’ random assignment to the network’s nodes. The performance of behavior-based-policies depends additionally on the particular realization of the simulated conjoint survey performed by the change prac-

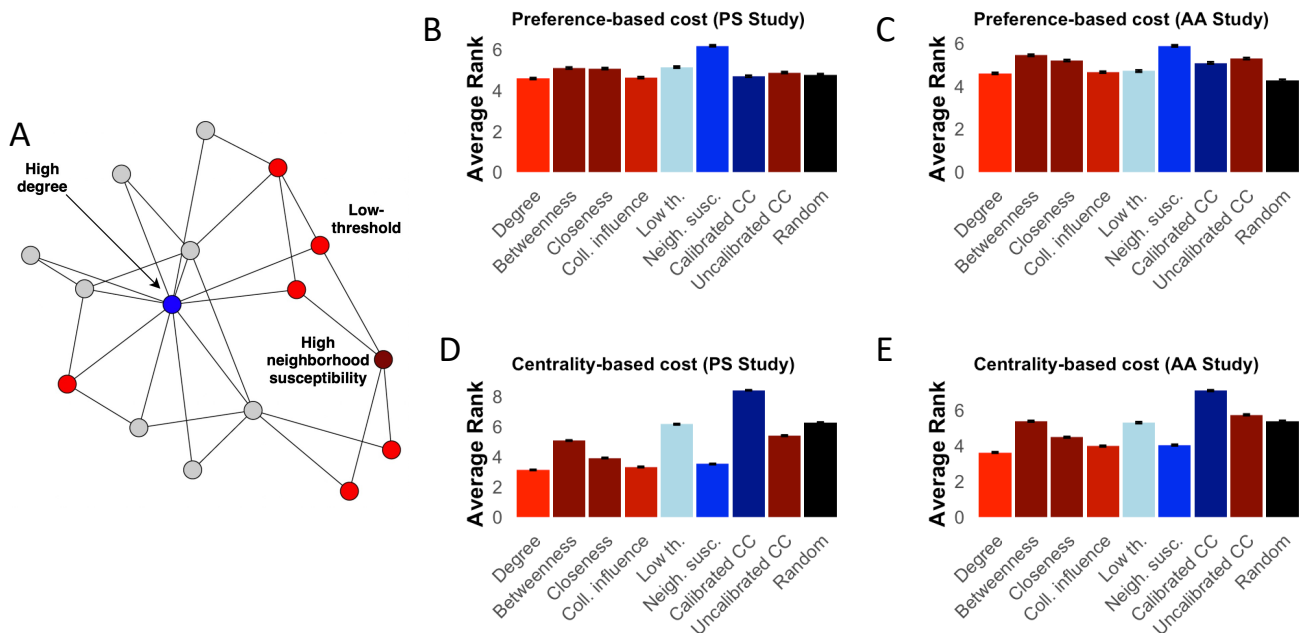


Fig. 2: **Relative performance of seeding policies.** (A) Nodes selected by different policies in an illustrative network structure: The highest-degree node (in blue) has the largest number of connections, but the highest-neighborhood susceptibility node (in dark red) has the largest number of connections to low-threshold nodes (in red). (B, C) Relative performance of seeding policies under a preference-based cost structure, measured through the average rank defined in the main text, for the policy support experiment and the app adoption experiment, respectively. The neighborhood susceptibility policy based on the estimated thresholds significantly outperforms the other policies. (D, E) Relative performance of seeding policies under a centrality-based cost structure for the policy support experiment and the app adoption experiment, respectively. The complex centrality policy based on the estimated thresholds significantly outperforms the other policies.

tioner to estimate the thresholds (see Supplementary Note S3). Note that in the language of disordered systems, for each network structure, both the ground-truth and the estimated thresholds of the nodes can be interpreted as quenched disorder variables [62] which we average our results over. For each configuration, we calculate the relative ranking position of the policies, which we subsequently average over all the configurations [63] to obtain the policies' mean rank showed in Fig. 2. In Supplementary Fig. S5, we show that the obtained results are robust with respect to an alternative relative performance measure for a given configuration, based on the ratio between a policy's performance and the best policy's performance [64] (see Methods).

We find that while there is no universally best-performing policy, the estimated thresholds are key to identifying the best-performing seeds. The relative performance of the policies critically depends on the structure of the cost function, but in all the analyzed scenarios, the best-performing policy is one that takes into account the estimated thresholds. Specifically, we first consider a cost function such that the cost to successfully initiate the spreading only depends on the seed nodes' preferences, but it is independent of the nodes' centrality (preference-based cost; see Methods). This scenario is especially rel-

evant to contexts where the seeds mostly adopt for personal motivations, and there is no reason why it would require more effort or monetary incentive to persuade central individuals to early adopt [19]. In these contexts, high-resistance individuals might require stronger interventions to be persuaded to initiate the spreading (e.g., more intervention cycles in a field intervention, or higher monetary incentives in marketing contexts; see Methods). We find that in the preference-based cost scenario, the neighborhood susceptibility policy significantly outperforms all the others (see Figs. 2B–C). Differences in performance between the neighborhood susceptibility and all other policies are significant ($p < 0.05$ for all one-tailed Wilcoxon signed-rank tests, see Methods). Through the estimated thresholds, the neighborhood susceptibility allows the identification of social neighborhoods that are more amenable to change and require a lower cost to successfully initiate the diffusion. Among the remaining policies, two network-based policies (betweenness and closeness) perform relatively well yet they underperform with respect to the neighborhood susceptibility. In this cost scenario, both the calibrated and the uncalibrated complex centrality perform similarly to the network-based policies.

The relative performance of the policies changes dra-

matically as we consider a different cost function such that the cost to target a node grows with the node’s centrality, independently of the node’s preferences (see Methods). This scenario is highly relevant to all those applications where there is a strategic advantage of initiating the diffusion from high-centrality nodes, which is often the case in online influencer marketing and other interventions where central nodes are highly sought-after because of their large follower bases and, therefore, are less responsive [65] and charge higher prices for endorsing new products [66–68]. We find that in the centrality-dependent cost scenario, the calibrated complex centrality significantly outperforms all the other policies (see Figs. 2D–E; the one-tailed Wilcoxon signed-rank tests between the calibrated complex centrality’s and all the other policies’ performances result in $P < 0.05$). This is due to its capability to identify low-degree nodes with high spreading capacity for complex contagions [41]. At the same time, the uncalibrated complex centrality – which neglects the estimated thresholds – fails to reach a similar performance. Therefore, the complex centrality is effective at identifying optimal seeds, but only if estimates of the individual-level thresholds are available to the social change practitioner. The network-based policies exhibit a lower performance than the random seeding policy. This confirms the argument that when the higher connectedness of high-degree nodes affects the seeding cost, the social hubs’ spreading ability might not be large enough to justify the extra efforts required to detect and target them [66]. In this scenario, only the calibrated complex centrality leads to consistently higher seeding performance.

Finally, we examine the relative performance of the seeding policies in scenarios where only a portion of the nodes have been surveyed, and a fraction of the thresholds is missing. As for the behavior-based policies, we narrow our focus to the low-threshold and neighborhood susceptibility policies. For simplicity, we assume that when selecting the seeds according to these two policies, the social change practitioner neglects completely information from the nodes that she has not been able to survey. Therefore in this scenario, the focal seed according to the low-threshold policy is the one with the lowest threshold among the surveyed nodes; the focal seed according to the neighborhood susceptibility policy is the one with the largest number of low-threshold neighbors among the surveyed nodes. We find that for both experiments, the neighborhood susceptibility policy maintains an advantage over the other policies as long as the large majority of the nodes (e.g., 90% or 75%) is surveyed (see Supplementary Figs. S10–S11). When data is highly incomplete (50% surveyed nodes or less), the advantage of the neighborhood susceptibility policy is still robust in the PS experiment, but not in the AA experiment (see Supplementary Figs. S12–S14). This is arguably due to the larger number of low-threshold nodes in the PS experiment, which makes the identification of low-threshold nodes simpler even with highly incomplete data. We

leave to future works the development of sophisticated techniques to improve the performance of behavior-based policies in scenarios with highly incomplete behavioral data.

Alternative social spreading theories

While the complex contagion theory captures many kinds of social spreading processes, alternative modeling approaches to collective adoption processes have been widely studied as well. We show here that broader classes of collective dynamical models can be reinterpreted in terms of individual-level choice models, which could open the way to new methods for their calibration against real data and inspire the development of new data-driven social dynamics models.

Simple contagion models depart from the complex contagion model above by assuming that one single exposure to a new product can be sufficient for an individual to adopt. The Bass model of new product diffusion is a paradigmatic simple contagion model [42, 69]. At each time step, an individual decides whether to adopt a new product or not according to the probability $\Pi_n = p_n + q_n s_n$, where p_n and q_n denote the well-known innovation and imitation coefficients [19, 42], respectively, and s_n denotes the social signal received by the individual about the product. We show that the Bass equation can be derived from individual-level utilities under the assumption that the utility from adopting depends linearly on the social signal, and there is a large stochastic component in the individual-level utility functions (see Supplementary Note S6 C). Under these assumptions, we find $p_n = 1/2 - R_n/T$ (the higher the resistance, the lower the innovation parameter) and $q_n = \gamma_n/T$ (the higher the marginal utility of the social signal, the higher the imitation coefficient). Here T is a “temperature” parameter that rules the relative weight of the stochastic and systematic components of the utility functions, which determines whether the adoption probability is consistent with a simple or a complex contagion model (see Supplementary Note S6). These findings suggest that individual-level models might benefit policies to maximize or prevent social spreading for a broader class of models than the complex contagion one studied in the main text.

Another important class of models that can be reinterpreted in terms of individual-level choice models include preferential attachment models, which capture the collective recognition received by cultural products such as books, scientific papers, and patents as well as individuals in social networks [70]. Differently from simple and complex contagion models, preferential attachment models do not capture the network propagation of new ideas and behaviors, but only the temporal evolution of their aggregate impact or popularity. By assuming that the individuals exhibit decreasing marginal utility from the aggregate social signal received about a product, we can derive several preferential-attachment models from

choice theory, including the original preferential attachment model [71] and its variants that incorporate node fitness [43, 72, 73] and homophily [74, 75] (see Supplementary Note S6 D). The proposed interpretation of preferential attachment models could inspire new methods for their calibration against empirical data [76, 77] as well as principled generalizations of the models to incorporate heterogeneous individual-level behaviors, which is largely unexplored in extant works.

DISCUSSION

To effectively steward collective behaviors in social systems, scholars from diverse disciplines [13, 18–21, 78] suggested the need for integrating individual-level behavioral models with simulations of collective behavior, but data-driven efforts in this direction remain rare. Our work contributes to such integration by developing a framework that connects collective models of social spreading with individual-level choice models. Within the complex contagion theory, we demonstrate how the proposed approach can be leveraged to estimate and validate individual-level thresholds for behavioral change, and to leverage the estimated thresholds to inform seeding policies aimed at initiating social change.

At the individual level, our experimental results indicate that once the thresholds are estimated, individual choices in out-of-sample tasks exhibit significant predictability. This finding not only provides a validation of the estimated thresholds, but might also inspire future studies aimed at improving the predictive power. Besides, knowing the estimated thresholds allowed us to disentangle an experimental choice context where most individuals choose independently of social signals from one where most individuals are susceptible to social influence. In future works, the threshold estimation procedure could be used to systematically identify which influence mechanisms and contexts cause social signals to play (or not play) a critical role in shaping individual choices, and what the best policy response could be.

Linking the individual and collective levels, our findings reveal the circumstances under which seeding policies that incorporate behavioral models can outperform traditional, network-based policies. For example, the recently-introduced complex centrality [41] identifies effective seeds only when the change practitioner has been able to collect individual threshold data, and the cost of successfully targeting a node grows with her network centrality. The simpler neighborhood susceptibility policy – relying on the number of susceptible neighbors a given node has – only outperforms the other methods when based on collected individual threshold data, and the cost of successfully targeting a node depends on her intrinsic preferences.

These findings indicate that in real contexts, therefore, successful seeding of a new product or behavior will require measuring the potential adopters’ preferences for

the product, their susceptibility to social influence, and understanding how the cost of successfully targeting an individual depends on her characteristics. Choice-based conjoint experiments – like those analyzed here – provide preference-measurement instruments which are simple to design, but they might be expensive to implement at scale (although our results show that robust results can be obtained even when only a fraction of the nodes is surveyed). At the same time, the individual-level choice framework developed here is not limited to data collected from choice-based conjoint surveys, and could in principle be adapted to any settings where historical choice data paired with social signals is available (e.g., from e-commerce platforms, social media, or field studies). Adapting the developed framework to the specifics of different data sources is a promising avenue for further research.

The boundaries to the effectiveness of the proposed framework deserve as well to be further investigated in future research. Our assumptions indicate that our main results hold if the timescale that governs the diffusion of the new product or behavior is significantly faster than the timescale that governs changes in individual-level preferences (i.e., thresholds) and network structure. This assumption is in line with state-of-the-art complex contagion and influence maximization works [16, 17, 22, 23]. In real complex social systems, however, stronger feedback loops may exist: collective diffusion outcomes, top-down interventions, and interactions between multiple diffusion processes can alter individual-level preferences. In some cases, preference changes could occur at similar timescales as diffusion processes [79]. Adapting our framework to these more complex scenarios and overall, determining the theoretical limits to the proposed approach remain fascinating challenges for future studies.

MATERIALS AND METHODS

Threshold estimation

We describe here the threshold estimation method, based on Eq. (1). Consider an individual n who needs to select a product from I alternatives. Each alternative $i \in \{1, \dots, I\}$ brings individual n a certain utility U_{ni} . In line with discrete choice theory [3], we assume that individual n chooses alternative i if and only if $U_{ni} > U_{nj}$, $\forall i \neq j$. The utility can be decomposed into an observable, systematic component (U_{ni}^*) and a random, unobserved component (ϵ_{ni}) such that $U_{ni} = U_{ni}^* + \epsilon_{ni}$. The probability that individual n chooses alternative i over j is $\text{Prob}(U_{ni} > U_{nj}) = \text{Prob}(\epsilon_{nj} - \epsilon_{ni} < U_{ni}^* - U_{nj}^*)$. Following the assumptions in main text, the systematic utility of individual n from adopting product i can be expressed as:

$$U_{ni}^* = \sum_{k=1}^K \beta_{nk} x_{ki} + \gamma_n s_{ni} \quad (2)$$

Under the assumption that ϵ_{ni} is i.i.d. Gumbel distributed, the model parameters (β_{nk} , γ_n) can be estimated from observed choices (e.g., in a choice-based conjoint experiment [50]) using a Hierarchical Bayes (HB) algorithm [49]. In this model, the probability of individual n to select an item i from a choice set is expressed as a multinomial logit whose parameters are estimated separately for each individual using Markov Chain Monte Carlo (MCMC) methods. In this work, we used the R package `ChoiceModelR` [80] for the HB estimation. See Supplementary Note S1 for more details on the estimation method used in the two experiments. The estimation yields individual-level estimates and thus allows to calculate the adoption threshold for every individual and every product.

Validation of estimated thresholds

We aim to assess the predictive power of the individual thresholds estimated from choice-based conjoint data. The core idea is to estimate the thresholds based on a training set, and quantify how many times, in the validation set, the participants make predictable choices, i.e., choices that do not contradict their threshold values. For each task in the survey, we fit the HB model (see previous paragraph) on a training set consisting of all tasks except one hold-out task and use the model to predict the choices in the validation set consisting of the hold-out task. We then calculate the average number of predictable choices over all the training-validation splits. Specifically, for a given choice task, we quantify the estimated appeal of product alternative i to participant n as $\hat{\Delta}_{ni} := s_i - \hat{\tau}_{ni}$, where s_i denotes the social signal displayed for alternative i and $\hat{\tau}_{ni}$ denotes the estimated threshold (based on the training set) of participant n for alternative i . The estimated appeal of the default alternative (nonadoption) is zero, as by definition, any product alternative would be more appealing than the default if the respective social signal would exceed the corresponding estimated threshold.

Formally, given that participant n selected alternative i^* in task \mathcal{Z}_z ($z \in \{1, \dots, Z\}$ with Z being the number of choice tasks) we say that compared to a different alternative $i \in \mathcal{Z}_z$, i^* is a predictable choice based on n 's estimated thresholds if $\hat{\Delta}_{ni^*} > \hat{\Delta}_{ni}$, where $\hat{\Delta}_{ni}$ denotes the estimated appeal of alternative i to participant n . As each task \mathcal{Z}_z has $I = 4$ alternatives (three products and one default option), we can measure the degree of predictability of n 's choice for task \mathcal{Z}_z as

$$a_{nz} = \frac{1}{I-1} \sum_{i \in \mathcal{Z}_z \setminus \{i^*\}} \Theta(\hat{\Delta}_{ni^*} - \hat{\Delta}_{ni}) \quad (3)$$

where the sum runs over the $I-1$ alternatives in task \mathcal{Z}_z that were not selected by n ; $\Theta(x) = 1$ if $x > 0$, $\Theta(x) = 0$ otherwise. Basically, an observed choice is perfectly predicted by the n 's estimated thresholds if none of its alternatives was more appealing according to the thresholds.

Pooling the predictability levels over all participants and over all training-validation splits (and considering there is only one hold out task in a validation set), we define the accuracy of the estimated thresholds as

$$A = \frac{1}{NZ} \sum_{n=1}^N \sum_{z=1}^Z a_{nz} \quad (4)$$

where N is the number of participants (and Z is the number of choice tasks in the experiment, here equal to the number of training-validation splits). Note that the accuracy function can be connected with the choice probabilities of a logit choice model in the limit of strong marginal utility of social signal: under the logit model (see Supplementary Note S6 B), in the limit $|\gamma| \gg 1$, one has indeed $P_{ni^*}/P_{ni} \simeq \Theta(\hat{\Delta}_{ni^*} - \hat{\Delta}_{ni})$.

Data-driven spreading simulations

We consider threshold-based spreading simulations where the agents' thresholds are set based on the experimental results. For the simulations, we set the ground-truth agents' thresholds to the values estimated in the two choice experiments. We additionally assume that the hypothetical decision maker has been able to survey the nodes of the network with a choice-based conjoint experiment. We simulate the answers of the agents in the conjoint experiment based on the individual-level utilities estimated in the choice experiments. We then proceed with the proposed threshold estimation procedure to estimate the thresholds (see Supplementary Note S3). We denote by τ_{ni} and $\hat{\tau}_{ni}$ the ground-truth and estimated threshold, respectively, of node n for product i . We simulate diffusion processes that unfold according to the same fractional threshold model studied by Ref. [41] using the ground-truth thresholds $\{\tau_{i\alpha}\}$.

We run the diffusion processes throughout the largest connected components of 18 empirical Add Health networks sampled from those analyzed by Guilbeault and Centola [41] (see Supplementary Note S2 A for the sampling procedure). For each network structure, we measure the nodes' centralities according to the degree, betweenness, closeness, and collective influence (see Supplementary Note S4 A). Besides, for each network structure, product, agent assignment realization, and realization of the simulated conjoint survey, we measure the behavior-based metrics defined in Supplementary Note S4, using the estimated thresholds $\{\hat{\tau}_{i\alpha}\}$ as input. We initiate the diffusion through a clustered protocol [41]: We activate both one focal node selected according to the centrality metrics, and a proportion of randomly-selected neighbors such that $z\% = 2.5\%$ of the nodes is initially active (if the focal seed node has not enough neighbors to reach this proportion of seeds, a recursive search on the higher-order neighbors is performed [41]; we also set a minimum seed set size of four nodes).

In the preference-based cost scenario, the cost of successfully seeding product α with the selected seed set, \mathcal{S} , is defined as $C_i(\mathcal{S}) = \sum_{n \in \mathcal{S}} \kappa_{ni}$, where $\kappa_{ni} = R_{ni}$ if $R_{ni} > 0$, $\kappa_{ni} = 0$ otherwise. This cost function embodies the idea that it is more costly to successfully target individuals with higher resistance to the product, and it can be derived through simple choice-theory arguments (see Supplementary Note S6 B). In the centrality-based cost scenario, the seeding cost is defined as $C_i(\mathcal{S}) = \sum_{n \in \mathcal{S}} k_n$, i.e., the cost of successfully seeding a node grows with her degree [65, 67, 68]. The performance of the seeding policy that targets seed set \mathcal{S} , $P_i(\mathcal{S})$, is assumed to be the final number of adopters, $A_i(\mathcal{S})$, discounted for the intervention's cost: $P_i(\mathcal{S}) = A_i(\mathcal{S})/C_i(\mathcal{S})$.

To assess the relative performance of the examined seeding policies, for each analyzed configuration \mathcal{C} , we rank the nine policies by their simulated performance. Here a configuration \mathcal{C} is identified by the network being analyzed, the product that spreads through the network, the agents' random assignment to the network's nodes, and the particular realization of the simulated conjoint survey performed by the change practitioner to estimate the thresholds. Therefore, for each configuration \mathcal{C} , each method m is assigned to a rank variable $r_m(\mathcal{C})$ (in case of ties, we assign the average of the ranks that would have been assigned without ties). We compare the methods' average rank across all configurations,

$$\bar{r}_m = \frac{1}{|\mathcal{C}|} \sum_{\mathcal{C}} r_m(\mathcal{C}), \quad (5)$$

as done in Friedman's statistical test [63]. We also consider an alternative metric where for each configuration \mathcal{C} , each method m is assigned to a performance variable that quantifies the method's performance compared to the best-performing method [64], $s_m(\mathcal{C}) = P_m(\mathcal{C})/\max_{m'}\{P_{m'}(\mathcal{C})\}$. Again, we average this variable over all configurations. For the best-performing policies in the preference-based cost scenario (i.e., the neighborhood susceptibility) and the centrality-based cost scenario (i.e., the calibrated complex centrality), we perform pairwise one-tailed Wilcoxon tests [41] between the ranks of the best-performing policy and those all the other policies, to ensure that the differences are statistically significant ($P < 0.05$).

Code and data availability

The code and data used to obtain the findings of this study will be made publicly available upon publication.

Author contributions

All authors conceived and designed the research; RA and RT conceived the use of conjoint analysis for the threshold estimation; RT implemented the choice experiments and performed the analysis of experimental data; MSM and RT performed the simulation analysis; all the authors analyzed data; MSM and RT wrote the first draft of the paper; all authors revised the paper.

Acknowledgements

This work has been supported by the URPP Social Networks and the Swiss National Science Foundation (Grant No. 100013-207888). We wish to thank Mingmin Feng for her detailed feedback on the code and the manuscript, and Luca Lazzaro and Tulasi Agnihotram for their help in conducting the conjoint studies and for their overall feedback provided in the process.

Additional information

Supplementary Information accompanies this paper.

Competing interests

The authors declare no competing interests.

Correspondence should be addressed to M. S. M. (manuel.mariani@business.uzh.ch).

- ¹Sara M Constantino, Gregg Sparkman, Gordon T Kraft-Todd, Cristina Bicchieri, Damon Centola, Bettina Shell-Duncan, Sonja Vogt, and Elke U Weber. Scaling up change: A critical review and practical guide to harnessing social norms for climate action. *Psychological Science in the Public Interest*, 23(2):50–97, 2022.
- ²Felix Creutzig, Leila Niamir, Xuemei Bai, Max Callaghan, Jonathan Cullen, Julio Diaz-José, Maria Figueroa, Arnulf Grubler, William F Lamb, Adrian Leip, et al. Demand-side solutions to climate change mitigation consistent with high levels of well-being. *Nature Climate Change*, 12(1):36–46, 2022.
- ³Kenneth E Train. *Discrete choice methods with simulation*. Cambridge University Press, 2009.
- ⁴Daniel Kahneman. *Thinking, fast and slow*. Macmillan, 2011.
- ⁵Joshua C Peterson, David D Bourgin, Mayank Agrawal, Daniel Reichman, and Thomas L Griffiths. Using large-scale experiments and machine learning to discover theories of human decision-making. *Science*, 372(6547):1209–1214, 2021.
- ⁶Jon Elster. *Explaining social behavior: More nuts and bolts for the social sciences*. Cambridge University Press, 2015.
- ⁷Mark Granovetter. Threshold models of collective behavior. *American Journal of Sociology*, 83(6):1420–1443, 1978.
- ⁸DJ Watts. A simple model of global cascades on random networks. *Proceedings of the National Academy of Sciences of the United States of America*, 99(9):5766–5771, 2002.
- ⁹John H Miller and Scott Page. Complex adaptive systems. In *Complex Adaptive Systems*. Princeton university press, 2009.
- ¹⁰Dirk Helbing, Dirk Brockmann, Thomas Chadeaux, Karsten Donnay, Ulf Blanke, Olivia Woolley-Meza, Mehdi Moussaid, Anders Johansson, Jens Krause, Sebastian Schutte, et al. Saving human lives: What complexity science and information systems can contribute. *Journal of Statistical Physics*, 158(3):735–781, 2015.
- ¹¹Jean-Philippe Bouchaud. Crises and collective socio-economic phenomena: simple models and challenges. *Journal of Statistical Physics*, 151:567–606, 2013.
- ¹²Alexander F Siegenfeld, Nassim N Taleb, and Yaneer Bar-Yam. What models can and cannot tell us about covid-19. *Proceedings of the National Academy of Sciences*, 117(28):16092–16095, 2020.
- ¹³Edward Bishop Smith and William Rand. Simulating macro-level effects from micro-level observations. *Management Science*, 64(11):5405–5421, 2018.
- ¹⁴Andrea Cavagna, Alessio Cimorelli, Irene Giardina, Giorgio Parisi, Raffaele Santagati, Fabio Stefanini, and Massimiliano Viale. Scale-free correlations in starling flocks. *Proceedings of the National Academy of Sciences*, 107(26):11865–11870, 2010.
- ¹⁵Manuele Brambilla, Eliseo Ferrante, Mauro Birattari, and Marco Dorigo. Swarm robotics: a review from the swarm engineering perspective. *Swarm Intelligence*, 7:1–41, 2013.
- ¹⁶Charles Efferson, Sonja Vogt, and Ernst Fehr. The promise and the peril of using social influence to reverse harmful traditions. *Nature Human Behaviour*, 4(1):55–68, 2020.
- ¹⁷Sinan Aral and Paramveer S Dhillon. Social influence maximization under empirical influence models. *Nature Human Behaviour*, 2(6):375–382, 2018.
- ¹⁸Joseph B Bak-Coleman, Mark Alfano, Wolfram Barfuss, Carl T Bergstrom, Miguel A Centeno, Iain D Couzin, Jonathan F Donges, Mirta Galesic, Andrew S Gersick, Jennifer Jacquet, et al. Stewardship of global collective behavior. *Proceedings of the National Academy of Sciences*, 118(27), 2021.
- ¹⁹Renana Peres, Eitan Muller, and Vijay Mahajan. Innovation diffusion and new product growth models: A critical review and research directions. *International Journal of Research in Marketing*, 27(2):91–106, 2010.
- ²⁰Mirta Galesic, Wändi Bruine de Bruin, Jonas Dalege, Scott L Feld, Frauke Kreuter, Henrik Olsson, Drazen Prelec, Daniel L Stein, and Tamara van Der Does. Human social sensing is an untapped resource for computational social science. *Nature*, 595(7866):214–222, 2021.
- ²¹Mirta Galesic, Henrik Olsson, Jonas Dalege, Tamara Van Der Does, and Daniel L Stein. Integrating social and cognitive aspects of belief dynamics: towards a unifying framework. *Journal of the Royal Society Interface*, 18(176):20200857, 2021.
- ²²Damon Centola and Michael Macy. Complex contagions and the weakness of long ties. *American journal of Sociology*, 113(3):702–734, 2007.
- ²³Douglas Guilbeault, Joshua Becker, and Damon Centola. Complex contagions: A decade in review. *Complex Spreading Phenomena in Social Systems*, pages 3–25, 2018.
- ²⁴Damon Centola. *How behavior spreads: The science of complex contagions*, volume 3. Princeton University Press Princeton, NJ, 2018.
- ²⁵Damon Centola. *Change: How to make big things happen*. Hachette UK, 2021.
- ²⁶Nicholas A Christakis and James H Fowler. The collective dynamics of smoking in a large social network. *New England Journal of Medicine*, 358(21):2249–2258, 2008.
- ²⁷Damon Centola. The spread of behavior in an online social network experiment. *Science*, 329(5996):1194–1197, 2010.
- ²⁸Sahiti Myneni, Kayo Fujimoto, Nathan Cobb, and Trevor Cohen. Content-driven analysis of an online community for smoking cessation: integration of qualitative techniques, automated text analysis, and affiliation networks. *American Journal of Public Health*, 105(6):1206–1212, 2015.
- ²⁹Sinan Aral and Christos Nicolaides. Exercise contagion in a global social network. *Nature communications*, 8(1):1–8, 2017.
- ³⁰Johan Ugander, Lars Backstrom, Cameron Marlow, and Jon Kleinberg. Structural diversity in social contagion. *Proceedings of the National Academy of Sciences*, 109(16):5962–5966, 2012.
- ³¹Jameson L Toole, Meeyoung Cha, and Marta C González. Modeling the adoption of innovations in the presence of geographic and media influences. *PLOS ONE*, 7(1):e29528, 2012.
- ³²Márton Karsai, Gerardo Iniguez, Kimmo Kaski, and János Kertész. Complex contagion process in spreading of online innovation. *Journal of The Royal Society Interface*, 11(101):20140694, 2014.
- ³³Emily Oster and Rebecca Thornton. Determinants of technology adoption: Peer effects in menstrual cup take-up. *Journal of the European Economic Association*, 10(6):1263–1293, 2012.
- ³⁴Lori Beaman, Ariel BenYishay, Jeremy Magruder, and Ahmed Mushfiq Mobarak. Can network theory-based targeting increase technology adoption? *American Economic Review*, 111(6):1918–43, 2021.
- ³⁵Daniel M Romero, Brendan Meeder, and Jon Kleinberg. Differences in the mechanics of information diffusion across topics: idioms, political hashtags, and complex contagion on twitter. In *Proceedings of the 20th International Conference on World Wide Web*, pages 695–704, 2011.
- ³⁶Vladimir Barash, Christopher Cameron, and Michael Macy. Critical phenomena in complex contagions. *Social Networks*, 34(4):451–461, 2012.
- ³⁷Clay Fink, Aurora Schmidt, Vladimir Barash, Christopher Cameron, and Michael Macy. Complex contagions and the diffusion of popular twitter hashtags in nigeria. *Social Network Analysis and Mining*, 6(1):1–19, 2016.
- ³⁸Daniele Notarmuzi, Claudio Castellano, Alessandro Flammini, Dario Mazzilli, and Filippo Radicchi. Universality, criticality and complexity of information propagation in social media. *Nature Communications*, 13:1308, 2022.
- ³⁹Sandra González-Bailón, Javier Borge-Holthoefer, Alejandro Rivero, and Yamir Moreno. The dynamics of protest recruitment through an online network. *Scientific Reports*, 1(1):1–7, 2011.
- ⁴⁰Zachary C Steinert-Threlkeld. Spontaneous collective action: Peripheral mobilization during the arab spring. *American Political Science Review*, 111(2):379–403, 2017.
- ⁴¹Douglas Guilbeault and Damon Centola. Topological measures for identifying and predicting the spread of complex contagions. *Nature Communications*, 12(1):1–9, 2021.
- ⁴²Frank M Bass. A new product growth for model consumer

- durables. *Management science*, 15(5):215–227, 1969.
- ⁴³Dashun Wang, Chaoming Song, and Albert-László Barabási. Quantifying long-term scientific impact. *Science*, 342(6154):127–132, 2013.
- ⁴⁴Rajeev Kohli and Vijay Mahajan. A reservation-price model for optimal pricing of multiattribute products in conjoint analysis. *Journal of Marketing Research*, 28(3):347–354, 1991.
- ⁴⁵Klaus M Miller, Reto Hofstetter, Harley Krohmer, and Z John Zhang. How should consumers’ willingness to pay be measured? an empirical comparison of state-of-the-art approaches. *Journal of Marketing Research*, 48(1):172–184, 2011.
- ⁴⁶Steven N Durlauf. How can statistical mechanics contribute to social science? *Proceedings of the national academy of sciences*, 96(19):10582–10584, 1999.
- ⁴⁷Jacob Goldenberg, Barak Libai, and Eitan Muller. The chilling effects of network externalities. *International Journal of Research in Marketing*, 27(1):4–15, 2010.
- ⁴⁸Everett M Rogers. *Diffusion of Innovations*. Simon and Schuster, 2010.
- ⁴⁹Greg M Allenby and Peter E Rossi. Hierarchical bayes models. *The handbook of marketing research: Uses, misuses, and future advances*, pages 418–440, 2006.
- ⁵⁰Vithala R Rao. *Applied conjoint analysis*. Springer Science & Business Media, 2014.
- ⁵¹Silvia Pianta, Adrian Rinscheid, and Elke U Weber. Carbon capture and storage in the united states: perceptions, preferences, and lessons for policy. *Energy Policy*, 151:112149, 2021.
- ⁵²Adrian Rinscheid, Silvia Pianta, and Elke U Weber. What shapes public support for climate change mitigation policies? the role of descriptive social norms and elite cues. *Behavioural Public Policy*, 5(4):503–527, 2021.
- ⁵³Abhijit Banerjee, Arun G Chandrasekhar, Esther Duflo, and Matthew O Jackson. The diffusion of microfinance. *Science*, 341(6144):1236498, 2013.
- ⁵⁴Flaviano Morone and Hernán A Makse. Influence maximization in complex networks through optimal percolation. *Nature*, 524(7563):65–68, 2015.
- ⁵⁵Linyuan Lü, Duanbing Chen, Xiao-Long Ren, Qian-Ming Zhang, Yi-Cheng Zhang, and Tao Zhou. Vital nodes identification in complex networks. *Physics Reports*, 650:1–63, 2016.
- ⁵⁶Eitan Muller and Renana Peres. The effect of social networks structure on innovation performance: A review and directions for research. *International Journal of Research in Marketing*, 36(1):3–19, 2019.
- ⁵⁷Christian Catalini and Catherine Tucker. When early adopters don’t adopt. *Science*, 357(6347):135–136, 2017.
- ⁵⁸Marcus Alexander, Laura Forastiere, Swati Gupta, and Nicholas A Christakis. Algorithms for seeding social networks can enhance the adoption of a public health intervention in urban india. *Proceedings of the National Academy of Sciences*, 119(30):e2120742119, 2022.
- ⁵⁹Jacob Goldenberg, Sangman Han, Donald R Lehmann, and Jae Weon Hong. The role of hubs in the adoption process. *Journal of Marketing*, 73(2):1–13, 2009.
- ⁶⁰Linton C Freeman. A set of measures of centrality based on betweenness. *Sociometry*, pages 35–41, 1977.
- ⁶¹Alex Bavelas. Communication patterns in task-oriented groups. *The Journal of the Acoustical Society of America*, 22(6):725–730, 1950.
- ⁶²Marc Mézard, Giorgio Parisi, and Miguel Angel Virasoro. *Spin glass theory and beyond: An Introduction to the Replica Method and Its Applications*, volume 9. World Scientific Publishing Company, 1987.
- ⁶³Milton Friedman. The use of ranks to avoid the assumption of normality implicit in the analysis of variance. *Journal of the American Statistical Association*, 32(200):675–701, 1937.
- ⁶⁴Fang Zhou, Linyuan Lü, and Manuel Sebastian Mariani. Fast influencers in complex networks. *Communications in Nonlinear Science and Numerical Simulation*, 74:69–83, 2019.
- ⁶⁵Andreas Lanz, Jacob Goldenberg, Daniel Shapira, and Florian Stahl. Climb or jump: Status-based seeding in user-generated content networks. *Journal of Marketing Research*, 56(3):361–378, 2019.
- ⁶⁶Duncan J Watts and Peter Sheridan Dodds. Influentials, networks, and public opinion formation. *Journal of Consumer Research*, 34(4):441–458, 2007.
- ⁶⁷Eytan Bakshy, Jake M Hofman, Winter A Mason, and Duncan J Watts. Everyone’s an influencer: quantifying influence on twitter. In *Proceedings of the Fourth ACM International Conference on Web Search and Data Mining*, pages 65–74, 2011.
- ⁶⁸Fine F Leung, Flora F Gu, Yiwei Li, Jonathan Z Zhang, and Robert W Palmatier. Influencer marketing effectiveness. *Journal of Marketing*, 86(6):93–115, 2022.
- ⁶⁹Gabriel Rossman and Jacob C Fisher. Network hubs cease to be influential in the presence of low levels of advertising. *Proceedings of the National Academy of Sciences*, 118(7):e2013391118, 2021.
- ⁷⁰Albert-László Barabási. *Network science*. Cambridge University Press, 2016.
- ⁷¹Albert-László Barabási and Réka Albert. Emergence of scaling in random networks. *Science*, 286(5439):509–512, 1999.
- ⁷²Ginestra Bianconi and A-L Barabási. Competition and multi-scaling in evolving networks. *EPL (Europhysics Letters)*, 54(4):436, 2001.
- ⁷³Matúš Medo, Giulio Cimini, and Stanislao Gualdi. Temporal effects in the growth of networks. *Physical Review Letters*, 107(23):238701, 2011.
- ⁷⁴Fragkiskos Papadopoulos, Maksim Kitsak, M Serrano, Marián Boguná, and Dmitri Krioukov. Popularity versus similarity in growing networks. *Nature*, 489(7417):537–540, 2012.
- ⁷⁵Fariba Karimi, Mathieu Géniois, Claudia Wagner, Philipp Singer, and Markus Strohmaier. Homophily influences ranking of minorities in social networks. *Scientific Reports*, 8(1):1–12, 2018.
- ⁷⁶Matúš Medo. Statistical validation of high-dimensional models of growing networks. *Physical Review E*, 89(3):032801, 2014.
- ⁷⁷Jan Overgoor, Austin Benson, and Johan Ugander. Choosing to grow a graph: modeling network formation as discrete choice. In *The World Wide Web Conference*, pages 1409–1420, 2019.
- ⁷⁸Frank Schweitzer. Sociophysics. *Physics Today*, 71(2):40–46, 2018.
- ⁷⁹Frances C Moore, Katherine Lacasse, Katharine J Mach, Yoon Ah Shin, Louis J Gross, and Brian Beckage. Determinants of emissions pathways in the coupled climate–social system. *Nature*, 603(7899):103–111, 2022.
- ⁸⁰Ryan Sermas. *ChoiceModelR: Choice Modeling in R*, 2022. URL <https://CRAN.R-project.org/package=ChoiceModelR>. R package version 1.3.0.
- ⁸¹Daniel McFadden. Conditional logit analysis of qualitative choice behavior. In Paul Zarembka, editor, *Frontiers in Econometrics*, pages 105–142. Academic press, New York, 1974.
- ⁸²Cbc questionnaires and design strategy, . URL https://legacy.sawtoothsoftware.com/help/lighthouse-studio/manual/hid_web_cbc_designs_1.html. Accessed on May 16th, 2024.
- ⁸³The basics of interpreting conjoint utilities, . URL <https://sawtoothsoftware.com/the-basics-of-interpreting-conjoint-utilities>. Accessed on April 19th, 2024.
- ⁸⁴Maren Hein, Peter Kurz, and Winfried J Steiner. Analyzing the capabilities of the hb logit model for choice-based conjoint analysis: a simulation study. *Journal of Business Economics*, 90(1):1–36, 2020.
- ⁸⁵Mark Newman. *Networks*. Oxford University Press, 2018.
- ⁸⁶Oliver Hinz, Bernd Skiera, Christian Barrot, and Jan U Becker. Seeding strategies for viral marketing: An empirical comparison. *Journal of Marketing*, 75(6):55–71, 2011.
- ⁸⁷Barak Libai, Eitan Muller, and Renana Peres. Decomposing the value of word-of-mouth seeding programs: Acceleration versus expansion. *Journal of Marketing Research*, 50(2):161–176, 2013.
- ⁸⁸Andrea Galeotti and Sanjeev Goyal. Influencing the influencers: a theory of strategic diffusion. *The RAND Journal of Economics*,

- 40(3):509–532, 2009.
- ⁸⁹Pablo Barberá, Ning Wang, Richard Bonneau, John T Jost, Jonathan Nagler, Joshua Tucker, and Sandra González-Bailón. The critical periphery in the growth of social protests. *PLOS ONE*, 10(11):e0143611, 2015.
- ⁹⁰Fang Zhou, Linyuan Lü, Jianguo Liu, and Manuel Sebastian Mariani. Beyond network centrality: Individual-level behavioral traits for predicting information superspreaders in social media. *National Science Review*, page nwae073, 2024.
- ⁹¹Gábor Csárdi, Tamás Nepusz, Vincent Traag, Szabolcs Horvát, Fabio Zanini, Daniel Noom, and Kirill Müller. *igraph: Network Analysis and Visualization in R*, 2024. URL <https://CRAN.R-project.org/package=igraph>. R package version 2.0.1.1.
- ⁹²Hema Yoganarasimhan. Impact of social network structure on content propagation: A study using youtube data. *Quantitative Marketing and Economics*, 10(1):111–150, 2012.
- ⁹³Matteo Marsili. On the multinomial logit model. *Physica A: Statistical Mechanics and its Applications*, 269(1):9–15, 1999.
- ⁹⁴Robert J MacCoun. The burden of social proof: Shared thresholds and social influence. *Psychological Review*, 119(2):345, 2012.
- ⁹⁵Graeme Blair, Rebecca Littman, and Elizabeth Levy Paluck. Motivating the adoption of new community-minded behaviors: An empirical test in nigeria. *Science Advances*, 5(3):eaau5175, 2019.
- ⁹⁶Sonja Vogt, Nadia Ahmed Mohammed Zaid, Hilal El Fadil Ahmed, Ernst Fehr, and Charles Efferson. Changing cultural attitudes towards female genital cutting. *Nature*, 538(7626):506–509, 2016.
- ⁹⁷Javier Borge-Holthoefer and Yamir Moreno. Absence of influential spreaders in rumor dynamics. *Physical Review E*, 85(2):026116, 2012.
- ⁹⁸Kyle W Higham, Michele Governale, Adam B Jaffe, and Ulrich Zülicke. Fame and obsolescence: Disentangling growth and aging dynamics of patent citations. *Physical Review E*, 95(4):042309, 2017.
- ⁹⁹Burcu Yucesoy, Xindi Wang, Junming Huang, and Albert-László Barabási. Success in books: a big data approach to bestsellers. *EPJ Data Science*, 7:1–25, 2018.
- ¹⁰⁰Andrea Capocci, Vito DP Servedio, Francesca Colaiori, Luciana S Buriol, Debora Donato, Stefano Leonardi, and Guido Caldarelli. Preferential attachment in the growth of social networks: The internet encyclopedia wikipedia. *Physical Review E*, 74(3):036116, 2006.
- ¹⁰¹Mark EJ Newman. Clustering and preferential attachment in growing networks. *Physical Review E*, 64(2):025102, 2001.
- ¹⁰²Matúš Medo, Manuel S Mariani, An Zeng, and Yi-Cheng Zhang. Identification and impact of discoverers in online social systems. *Scientific Reports*, 6(1):34218, 2016.
- ¹⁰³Freda B Lynn, Joel M Podolny, and Lin Tao. A sociological (de) construction of the relationship between status and quality. *American Journal of Sociology*, 115(3):755–804, 2009.
- ¹⁰⁴Shilpa Ghadge, Timothy Killingback, Bala Sundaram, and Duc A Tran. A statistical construction of power-law networks. *International Journal of Parallel, Emergent and Distributed Systems*, 25(3):223–235, 2010.
- ¹⁰⁵Michael Golosovsky. Mechanisms of complex network growth: Synthesis of the preferential attachment and fitness models. *Physical Review E*, 97(6):062310, 2018.

Supplementary Material for:

Integrating behavioral experimental findings into dynamical models to inform social change interventions

Radu Tanase, René Algesheimer, Manuel Sebastian Mariani

CONTENTS

Results	2
From individual-level preferences to complex contagion	2
Experimental validation	3
Detection of independent and susceptible individuals	4
Implications for seeding policies	5
Alternative social spreading theories	7
Discussion	8
Materials and Methods	8
Threshold estimation	8
Validation of estimated thresholds	9
Data-driven spreading simulations	9
S1. Choice-based conjoint experiment	15
A. Brief introduction to choice-based conjoint experiments	15
B. The policy support study (PS)	15
C. The app adoption study (AA)	19
S2. Data for the data-driven simulations	22
A. Social network data	22
B. Product sampling	22
S3. Simulated conjoint survey to inform seeding policies	22
A. Survey simulation	22
B. Parameter recovery	23
S4. Seeding policies	23
A. Network-based seeding policies	23
B. Behavior-based seeding policies	23
S5. Additional results for seeding policies	25
A. Results for the ratio-to-best metric	25
B. Results for different seed set sizes	26
C. Results in scenarios with partial threshold data	30
S6. Linking individual-level choice models with social spreading theories	33
A. Linking individual utilities and adoption probabilities	33
B. Complex contagion theory	33
C. Simple contagion: Bass model	34
D. Preferential attachment and fitness models	35

S1. CHOICE-BASED CONJOINT EXPERIMENT

A. Brief introduction to choice-based conjoint experiments

Conjoint experiments are a widely-used technique [50] to measure how the total evaluation of a product or behaviour (further referred as product) is related to the aspects describing the product (further referred as product attributes). Choice-based conjoint experiments (CBC) are a specific type of conjoint experiments where the product evaluation is done in terms of a discrete choice. Specifically, participants in CBC experiments are faced with a number of choice tasks. In each choice task, participants are presented a number of products (i.e., choice alternatives) which differ along several dimensions (i.e., product attributes) and are asked which one they would choose (if any) in a given (often hypothetical) situation. From observing such choices, it is then possible to infer which product attributes individuals value most in making the decision. This builds on the premise that when making the choice, participants trade-off different aspects of the choice alternatives.

The theoretical foundation for CBC lies in the random utility theory [81]. In such models, an individual is faced with a number of choice alternatives in a choice set, each bringing her a certain utility. The individual will choose the alternative with the highest utility. While the utility of each alternative is known to the individual, it is not known to the researcher. Therefore, from the researcher’s point of view, an individual’s (random) utility can be decomposed into a deterministic part and a random component [3]. The deterministic part is a function (often a linear combination) of the utility corresponding to each product attribute (i.e., partworth utilities or simply attribute utilities). The random component is unknown and requires some assumptions about its distribution. These assumptions determine which model will be used to describe the probability that a product is chosen. The most used model is the multinomial logit, which assumes the random component follows an extreme value distribution [50].

The Hierarchical Bayes (HB) model [49] (used in this article) is a variation of the multinomial logit that yields individual-level estimates of the attribute utilities (i.e., one estimate for each individual and each level of any product attribute). Based on the individual level estimates, it is then possible to calculate the total utility of a product for an individual. The HB model assumes that the individual partworth utilities follow the same distribution for all the individuals in the sample, with the distribution’s parameters drawn from a population distribution. To estimate the partworth utilities, it first assumes an initial value of the parameters describing the distribution (i.e., prior belief) and then updates it based on data in a Bayesian manner. As the resulting equations cannot be solved analytically, the estimation is done using Markov Chain Monte Carlo (MCMC) methods [49, 50]. We refer the interested reader to ref. Rao [50] for an applied introduction into conjoint analysis and to ref. Train [3] for a comprehensive read which includes extensive details into how various models are formulated and estimated.

B. The policy support study (PS)

Study design and data. We recruited 296 US participants (300 participants in total, but 4 participants have been excluded for not completing the survey) from a demographically (i.e., gender and ethnicity) representative US sample on Prolific to take part in a choice-based conjoint survey on support for carbon capturing policies. Participants were told to imagine a carbon capture and storage policy might be implemented in their state and they need to select which alternative from a choice set they would endorse. Each choice set contained three policies and a none option. The policies presented were described by five attributes (policy type, policy costs, beginning of the policy implementation, required distance to residential areas and organisation endorsing the policy) with four levels each, closely following Pianta et al. [51]. Additionally, we included a sixth attribute representing the (hypothetical) percentage of one’s friends who endorse the policy. Participants were presented with a total of 15 choice tasks, each participant receiving a different set of choice tasks (generated by the Sawtooth software using the balanced overlap method [82]). An overview of the attributes and levels used in the conjoint design can be seen in Table S1. A sample of the conjoint survey administered to the participants is attached to this Supplementary Material.

Estimation. We estimated the individual partworth coefficients using the Hierarchical Bayes [49] algorithm. We used the function `choicemodelr` from the R package `ChoiceModelR` [80] with 30’000 MCMC iterations (10’000 for burn in and the remaining 20’000 for parameter estimation). We considered the attribute *Percentage of friends who endorse the policy* as numeric and the remaining attributes (including the none option) as categorical, for which we used effects coding. Note that in effects coding all levels of a variable represent deviations from the overall mean (as opposed to a specific reference level when using dummy coding) with the constraint that all levels sum to zero. For the none option, the effects coding implies we have one level for choosing the status quo (`none=True`) and one level for choosing any of the alternatives in the choice set (`none=False`). We note that in computing the utility of an alternative in the choice set, the value of `none=False` needs to be added to (the sum of) the utilities of the attributes describing

Attributes	Levels				
Policy type	Ban	Subsidies	Tax		
Policy costs	\$4	\$9	\$14	\$19	
Beginning of policy implementation	2025	2035	2045	2055	
Required distance to residential areas	2 miles	5 miles	10 miles	50 miles	
Policy endorsement by	Carbon Capture Coalition	Greenpeace	Democratic Party	Republican Party	
% of your friends who endorse the policy scenario	1%	23%	45%	76%	98%

TABLE S1: **Attributes and levels used in the Carbon Capturing Policy Study.**

the alternative. Thus individual n 's utility from adopting product (or behavior) i is $U_{ni} = U_{ni}^{(A)} + U_{ni}^{(S)} + U_n^{(0)}$, where $U_n^{(0)}$ is the utility corresponding to `none=False`. As this is just an artifact of the coding system used in estimation, we referred everywhere in the text to U_{ni} as $U_{ni} = U_{ni}^{(A)} + U_{ni}^{(S)}$, which correspond to a dummy coding of the none option. The HB algorithm does not directly result in point estimates (single values of a parameter) but rather in a distribution of values for each parameter (one value being generated in each MCMC draw used for parameter estimation). Therefore, we calculated the parameter estimates as the sample mean of the distribution of the MCMC draws. We input the resulting estimated parameters ($\hat{\beta}_n, \hat{\gamma}_n, \hat{U}_n^{(0)}$) into Eq 1 in main text to obtain the estimated threshold for product i .

Model quality. First, we measured the reliability of the conjoint data by including two fixed choice tasks (on positions 5 and 10) that were identical within respondents, and measured how many respondents gave the exact same answer to both tasks [45]. We found the answers to the two questions were the same for 77% of the respondents, which is substantially larger than the expected fraction (25%) in a baseline model where individuals make decisions at random.

Second, we evaluated how well the model predicts choices out of sample. To this end, we split the data into a held-out test set consisting of one choice task and a training set consisting of the remaining choice tasks¹. We fitted the model only on the training set, predicted the choices in the test set, and compared the predictions against the observed choices. We repeated this process for all choice tasks. We found an average out of sample accuracy rate of 66%, which is significantly larger than the accuracy rate of a baseline model making choices at random (25%, as each task consists of 3 policy alternatives + a none option).

Results. We assess the impact of each attribute on the respondents' choices by measuring the attributes' relative importance. To measure the attribute importance for an individual, we measure for each attribute a , the difference between the maximum and minimum marginal utility across all levels of a . We normalize the obtained attribute importance values so that they sum to one for each individual. To obtain the results in Table S2, we subsequently average the obtained individual attribute importance values over all individuals [83]. We found the attribute with the highest relative importance is the beginning of policy implementation, followed by policy costs, required distance to residential areas, organisation endorsing the policy, percentage of friends endorsing the policy, and policy type (see Table S2). On average, cheaper, stringent (ban) policies that start soon and are further away from the residential area are more appealing than expensive, lax policies that start late and close to the residential area (see Fig. S1). The ranking of the attribute level utilities within the same attribute are largely consistent with the study we draw from [51], the only difference being in the ranking of organisations endorsing the policy. We observe that 290 out of the 296 valid respondents have a positive partworth utility of the social signal (with the remaining 6 having a negative value). We note that an interpretation of the individual-level threshold is only compatible with the social contagion literature if the partworth utility of the social signal is not negative, which is true for almost all respondents. We remove from our analysis the 6 respondents with a negative partworth utility of the social signal, and leave the study of these special cases to further research. We measure the individual-level thresholds using the methodology described in the Methods section of the article for the 36 sampled products (see Supplementary Note S2B) and calculate the average threshold per product. The results can be seen in Figure S2.

¹ To avoid data leakage (i.e., information from the test set leaking into the training set), we removed the second fixed choice task from the data. As there are two identical fixed tasks, removing

one of them is essential to avoid that the same task is present in both the training and test sets.

Variable	Average Importances	Standard Deviation
Beginning of policy implementation	0.2058795	0.14133569
Policy costs	0.1792849	0.11280490
Required distance to residential areas	0.1627719	0.09508369
Policy endorsement by	0.1585160	0.08416735
% of your friends who endorse the policy scenario	0.1477991	0.08915445
Policy type	0.1457485	0.09594621

TABLE S2: **Average variable importance in the Carbon Capturing Policy Study.** The most important is beginning of policy implementation, followed by policy costs, required distance to residential areas, organisations who endorses the policy scenario, percentage of friends who endorse the policy scenario and policy type.

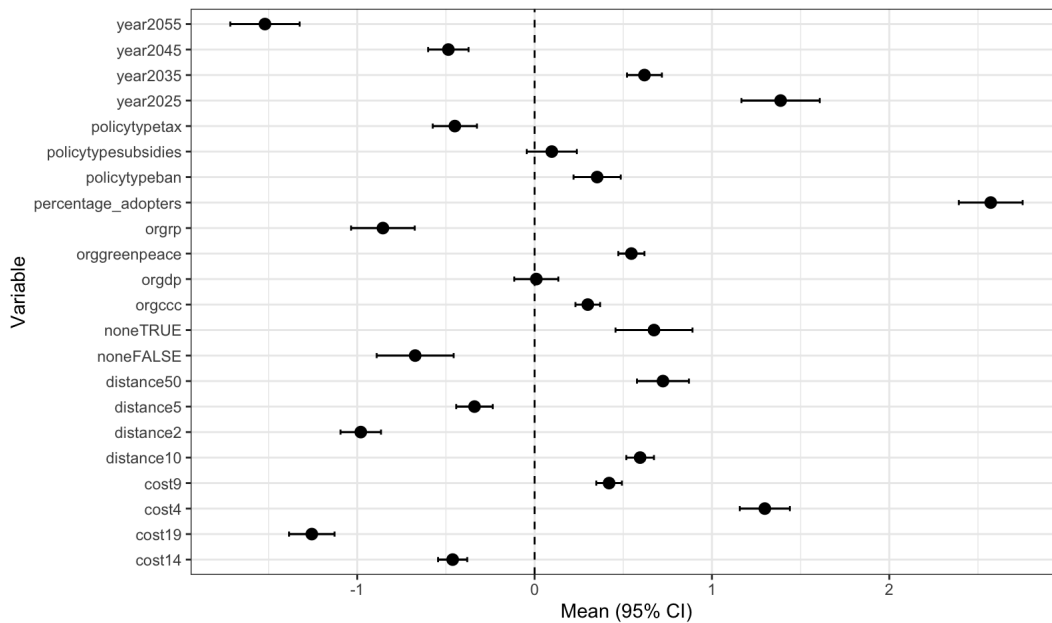


Fig. S1: **Average utilities across respondents.** The y axis contains all attributes and levels. The x axis shows the average utility of an attribute level together with the 95 % confidence interval. On average, the percentage of friends endorsing the policy (labeled as *percentage_adopters*) has a positive partworth utility.

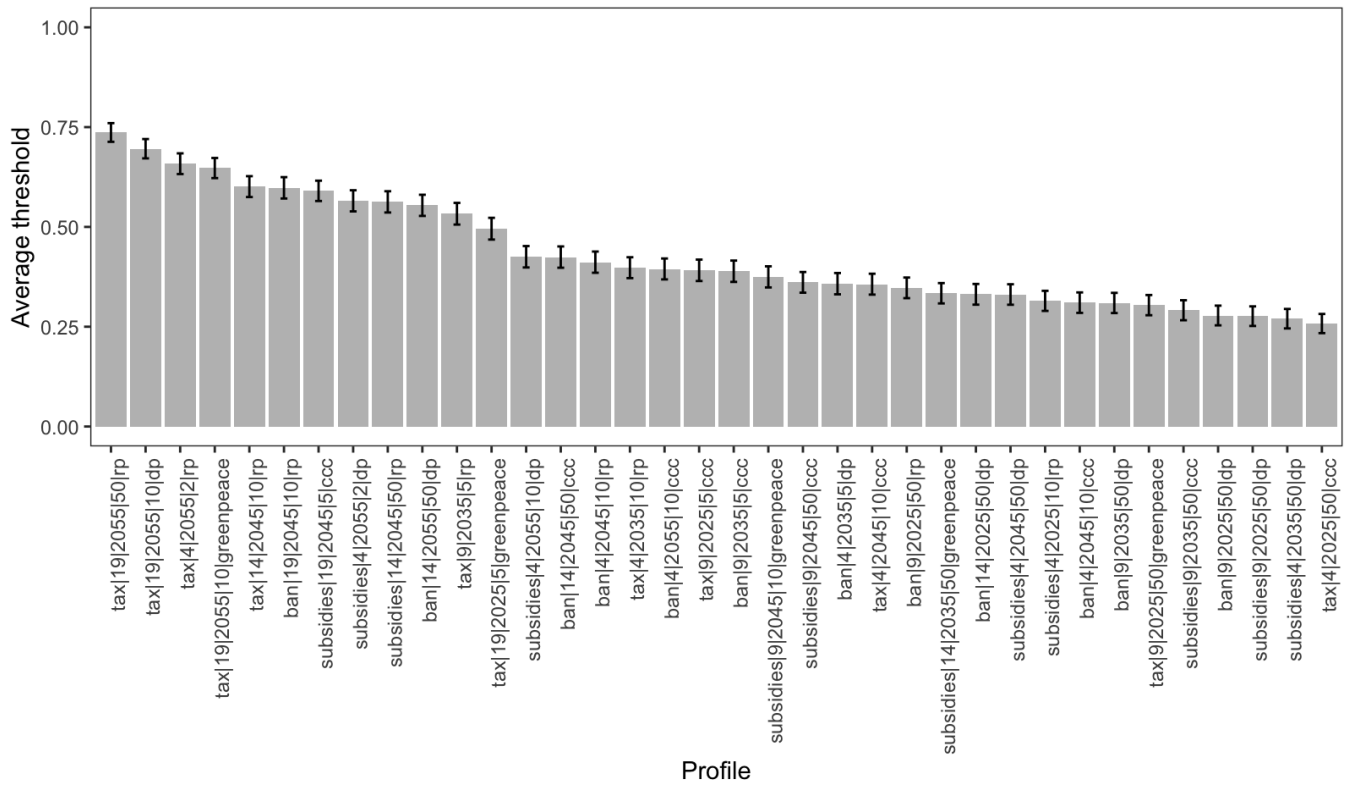


Fig. S2: **Average threshold over individuals (y axis) for each policy (x axis)**. The error bars represent the 95% confidence intervals for the mean. The policies are sorted by the average threshold. We observe that some policies have a lower average threshold, which implies that they are more attractive to the respondents.

Attribute	Level				
Accessibility	Mobile	Web			
Authentication	Simple	Two-factor	Multi-factor		
Customisation level	Low	Medium	High		
Video calls	Multi-person	One-to-one			
% of your friends already using the app	1%	23%	45%	76%	98%

TABLE S3: Attributes and levels used in the App Adoption Study.

C. The app adoption study (AA)

Study design and data. In this study, we surveyed respondents about their use of a new instant messaging applications. The setup was identical to the PS study. We recruited 300 US participants from Prolific (54% female). The (fictive) messaging apps were described by four attributes (accessibility, authentication, customisation level and video call support) with two to three levels each. Similarly to the PS Study, we included a fifth attribute representing the (hypothetical) percentage of one’s friends who are already using the app. Participants were presented with a total of 14 choice tasks, each participant receiving a different set of choice tasks (generated by the Sawtooth software using the balanced overlap method [82]). An overview of the attributes and levels used in the conjoint design can be seen in Table S1. A sample of the conjoint survey administered to the participants is attached to this Supplementary Material.

Estimation. We used again Hierarchical Bayes with 30’000 MCMC iterations, the first 10’000 for burn in and the remaining 20’000 for parameter estimation. We considered the attribute *Percentage of friends already using the app* as numeric and the remaining attributes as categorical, for which we used effects coding. We calculated the parameter estimates as the sample mean of the distribution generated by the MCMC draws.

Model quality. To evaluate the model quality we performed the out of sample prediction validity test described in the PS Study. We found an average prediction accuracy of 71% which is substantially larger than that of a baseline model making choices at random (25%, as before).

Results. Overall, compared to the PS study, we find higher variation in average importance between the attributes. The highest ranked attribute is the percentage of friends already using the app, followed by accessibility, authentication, customisation level, and video calls (see Table S4). On average, messaging apps that are also web accessible, have two or multi-factor authentication and have a medium-high level of customisation are more appealing than mobile only apps with simple authentication and low customisation level (see Fig. S3). We observe that 299 out of the 300 respondents have a positive partworth utility of the social signal, with the remaining one having a negative utility. For the reasons outlined in describing the PS study, we did not consider further in the analysis the participant with a negative partworth utility of the social signal.

Variable	Average Importance	Standard Deviation
% of friends already using the app	0.57058823	0.15637008
Accessibility	0.13263729	0.11812613
Authentication	0.12093168	0.07900124
Customisation level	0.10435697	0.06559861
Video calls	0.07148583	0.05902997

TABLE S4: Average variable importance in the App Adoption Study. The variables are ranked by importance.

We measure the individual-level threshold using the methodology described in the Methods section of the article and calculate the average threshold per product. The results can be seen in Figure S4.

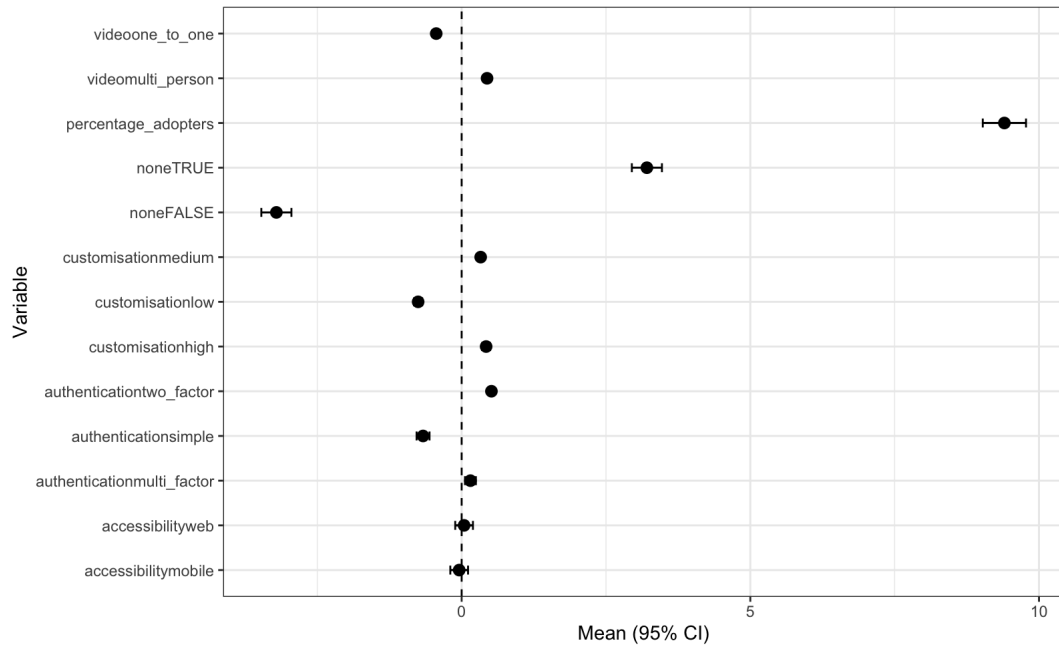


Fig. S3: **Average utilities across respondents.** The y axis contains all attributes and levels. The x axis shows the average utility together with the 95 % confidence interval. We can see that on average, the percentage of adopters has a large, positive utility.

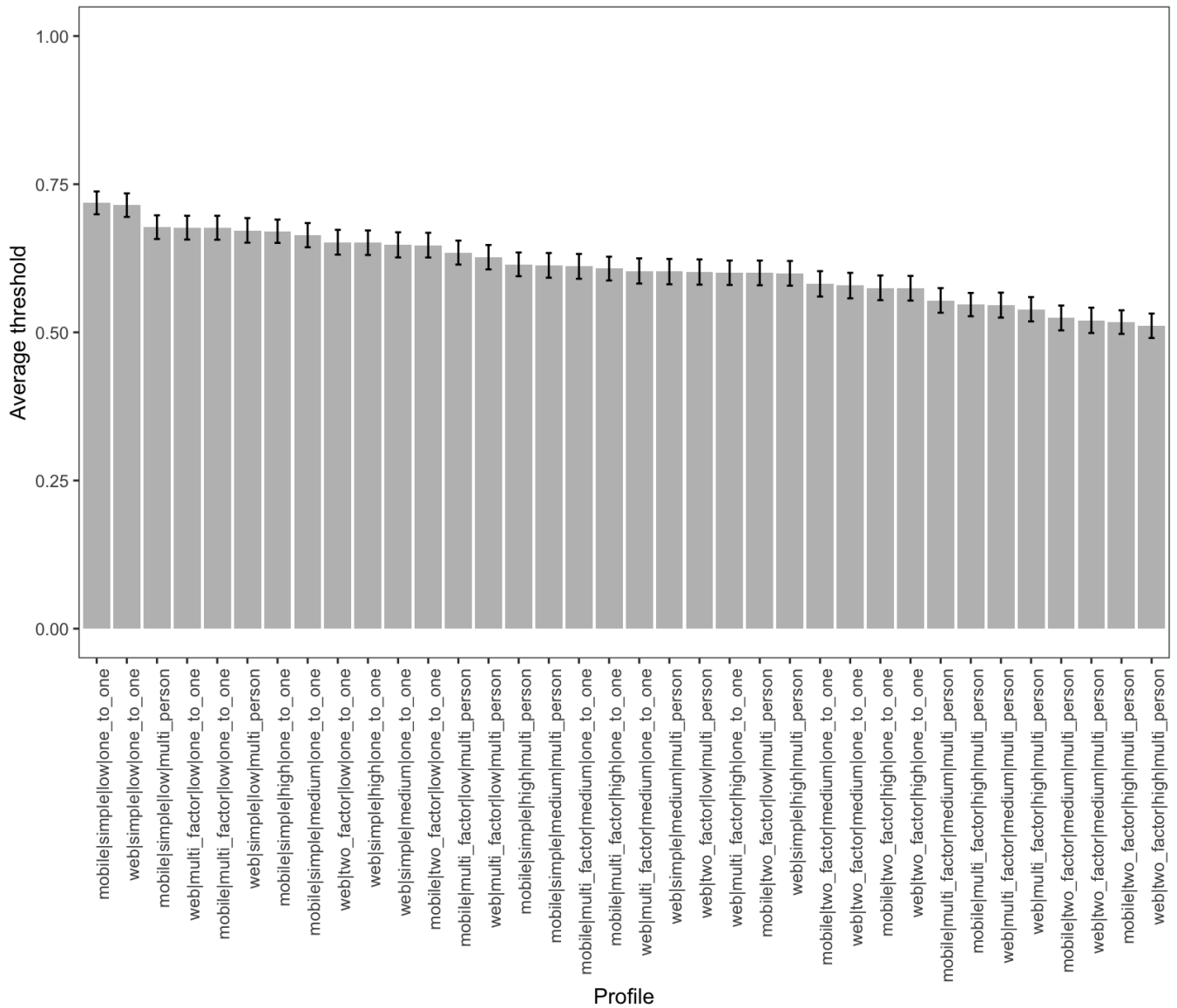


Fig. S4: **Average threshold over individuals (y axis) for each product (x axis)**. The error bars represent the 95% confidence intervals for the mean. The products are sorted by the average threshold. We can observe some products have a lower average threshold, implying they are more attractive. However, compared to the PS Study, the difference between the most and the least attractive product is considerably smaller.

S2. DATA FOR THE DATA-DRIVEN SIMULATIONS

A. Social network data

The original Add Health data [41] contains 85 networks. To save computational time, we restrict the analysis to a sample of 18 networks spanning diverse network properties. We constructed the sample as follows. For every network, we computed the number of nodes and the global transitivity index of the graph (i.e., the number of observed transitive triads divided by the number of potential transitive triads [70]). For each of the two metrics, we computed the 33% and 67% quantiles and labelled each network with respect to the metric as: low (metric < 33% quantile), medium (metric lies between the 33% and the 67% quantiles) or high (metric > 67% quantile). In this way, each network received two labels, one for the number of nodes and the other for transitivity. We created all possible combinations of the two labels (9 in total) and sampled two networks from each combination.

B. Product sampling

The total number of products that can be generated from a conjoint design is equal to all distinct combinations of attribute levels (not considering the social signal). Thus, there are 768 and 36 possible products in the PS and AA study, respectively. To save computational time, we decided to restrict our analysis to: (1) all 36 products in the AA study and (2) a subset of 36 products from the PS study. We selected the 36 products from the PS study such that the average threshold over respondents per product spans a broad range of observed values. Specifically, we calculated the threshold of every respondent for every product as described in the Methods section in the main text. Then we calculated the average threshold per product over respondents. We divided the range of the average threshold values in 6 equally-sized intervals (based on the 16.7%, 33%, 50%, 67% and 83% quantiles) and sampled 6 products from each interval.

S3. SIMULATED CONJOINT SURVEY TO INFORM SEEDING POLICIES

A. Survey simulation

We consider a scenario where a change practitioner needs to estimate individual thresholds to inform behavior-based seeding policies. As explained in the main text, we initially assume that the change practitioner has been able to survey the nodes of the network. For our simulation study, we simulate this survey. To simulate the survey, we follow a three step procedure, similar to the one described in Hein et al. [84]: (1) We calibrate the agent’s partworth utilities on the empirical data from the two conjoint experiments (PS and AA); (2) We generate choice tasks; (3) We simulate agents’ choices in the choice tasks based on their partworth utilities. To ensure that our results do not depend on a specific realization of the data, we generate 5 independent choice datasets for each of the two empirical conjoint studies (PS and AA) following the procedure below.

1. *Calibration of partworth utilities.* Each agent is characterised by an n_{par} -dimensional vector whose elements constitute the partworth utilities. Thus $n_{par} = 24$ in the PS study and $n_{par} = 13$ in the AA study (one parameter for each level of each attribute, one parameter for the social signal, and two parameters for the none option). We set the agents’s vector of partworth utilities equal to the ones estimated from the focal conjoint study (see Supplementary Note S1 for the estimation details).

2. *Generation of choice tasks.* We generate 15 choice tasks per agent, each with a choice set consisting of two product alternatives and a none option. Each product alternative in the choice set is described as a unique combination of the product attributes from the focal conjoint study, and one out of three levels of the social signal: 0.1, 0.5 or 0.9. For every agent and every choice set, we randomly sample the two alternatives from the set of all possible product configurations.

3. *Choice simulation.* We simulate the conjoint survey by simulating the choices made by the agents. To simulate which alternative was selected in each choice set, we compute the utilities corresponding to each alternative, and the utility of the none option. For each agent, we compute the utility of a given alternative by summing up the attribute utilities for that alternative and the utility of the social signal corresponding to the given social signal level. We assume the utility of the none option is constant within each agent across choice tasks. We further assume there is some noise in the process (as for example when the attributes included in the conjoint are not sufficient to fully capture the total utility of a product) and add to the utility of each alternative (either product or none) a random component drawn from a Gumbel distribution with scale parameter $\theta = 1$ [84]. Lastly, we assume that the agent

selects the alternative with the highest total utility. The resulting choice dataset contains 300 agents with 15 choice tasks each.

B. Parameter recovery

For each simulated choice dataset we recover the individual partworth utilities using the Hierarchical Bayes algorithm (similarly to what we did in the two real conjoint studies, see Supplementary Note S1). We used 30'000 MCMC iterations, the first 10'000 for burn in and the remaining 20'000 for parameter estimation. We considered the social signal attribute as numeric and the remaining attributes as categorical, for which we used effects coding. We calculated the parameter estimates as the sample mean of the distribution generated by the MCMC draws. We used the estimated parameters to calculate the estimated thresholds through Eq.(1) in the main text.

We tested the quality of the parameter recovery in two ways, similarly to Hein et al. [84]. First, we calculated the mean Pearson correlation between the ground-truth and the estimated partworth utilities over all agents. As the average of Pearson correlations does not converge to the true correlation, following Hein et al. [84], we first rescaled the correlation coefficients using Fisher's z -transformation [$f(x) = 0.5 \log((1+x)/(1-x))$], averaged the rescaled correlations, and converted the resulting average back to the original scale using the inverse of Fisher's z -transform. We found the mean correlation ranges over simulated datasets from 0.74 to 0.75 in the PS study and from 0.72 to 0.75 in the AA study.

Second, we measured how often the true coefficients lie within the 95% credible intervals of the estimated coefficients. We found this value ranges over simulated datasets from 94.97% to 95.85% in the PS study and from 94.69% to 96.00% in the AA study. As the average correlation coefficients are large and the true coefficients lie almost always within the 95% credible intervals of the estimated coefficients, we conclude the parameter recovery is accurate.

S4. SEEDING POLICIES

A. Network-based seeding policies

Degree policy. The degree assumes that a node is central if she has many connections. A node's degree is simply defined as its number of connections [85]. Despite the simplicity of this metric, some works have found high-degree nodes to be effective at predicting and triggering large-scale cascades of adoptions [59, 86, 87], although some works found counterexamples in model-based and empirical data, e.g., [66, 88–90]. We compute it via the `igraph` package [91].

Betweenness policy. The betweenness centrality assumes that a node is central if she is traversed by many of the network's shortest paths. For a focal node i , it averages over all pairs of nodes (s, t) the fraction of shortest paths between s and t that pass through i [85]. Similarly to high-degree nodes, some works have found high-betweenness nodes to be effective at triggering large-scale cascades of adoptions [86], although some works found counterexamples in model-based and empirical data, e.g., [69, 92]. We compute it via the `igraph` package [91].

Closeness policy. The closeness centrality assumes that a node is central if it is close to many other nodes in the network. It is defined as the inverse of the sum of shortest-path distances from the focal node to all the other nodes in the network [61]. Some works have found high-closeness nodes to be effective at triggering large-scale cascades of adoptions, especially for simple contagions above their critical point [64]. We compute it via the `igraph` package [91].

Collective Influence policy. The collective influence metric is derived analytically as an approximate solution to a network dismantling problem. In this problem, one seeks to find the minimal set of nodes whose removal from the network causes the collapse of the network's largest component [54]. We compute it via our own function.

B. Behavior-based seeding policies

For each configuration \mathcal{C} (identified by the network being analyzed, the product that spreads through the network, the agents' random assignment to the network's nodes, and the particular realization of the simulated conjoint survey performed by the change practitioner to estimate the thresholds), we measure various node-level behavior-based metrics that take into account the estimated thresholds (see main text and Supplementary Note S3). The underlying assumption is that the social change practitioner has been able to survey the nodes of the network, estimate their thresholds for different products, and use the estimated thresholds to implement the seeding policies defined below.

Low threshold policy. The low-threshold policy simply selects as the focal seed the node with the lowest estimated threshold in a given configuration; In case of ties, the focal node is selected at random among those with the lowest estimated threshold.

Neighborhood susceptibility policy. The neighborhood susceptibility (NS) of a given node i is defined as her number of low-threshold (highly-susceptible) social contacts. Following Watts [8], we define a given node j is a low-threshold node if $\hat{\tau}_j \leq k_j^{-1}$, where $\hat{\tau}_j$ is the threshold estimated by the social change practitioner and k_j is the degree of node j ; if this is the case, a single adoption event in j 's neighborhood is sufficient to trigger her adoption. Therefore, high-NS nodes are not necessarily the most central ones in the network according to the degree, but they are surrounded by a local "mass" of highly-susceptible individuals. Differently than the degree and other standard centrality metrics, the NS metrics takes into account individual-level behavioral information, namely, individuals' thresholds.

Calibrated and uncalibrated complex centrality (CC) policies. The complex centrality metric has been introduced by Guilbeault and Centola [41] to identify the optimal network locations where to initiate a complex contagion process under a clustered seeding strategy. In Guilbeault and Centola [41]'s code, the complex centrality metric is measured by running the simulation of the complex contagion process under the ground-truth thresholds, and then measuring the number of shortest paths that traverse a node in the "activated network" composed of the nodes who adopted. We adapt their code to our study by measuring the complex centrality based not on the ground-truth thresholds (which are typically unknown to the decision maker), but on different assumptions on which individual-level behavioral data is available to the social change practitioner. For simplicity, we consider here two scenarios.

- *Calibrated complex centrality (CCC).* We assume that the change social practitioner has been able to survey the network's nodes, and uses the estimated thresholds to run the simulations behind the complex centrality calculation.
- *Uncalibrated complex centrality (UCC).* We assume that the change practitioner has no behavioral information about the network's nodes. Following the same procedure used by Guilbeault and Centola [41] in their analysis of Indian villages, we average each node's complex centrality over an ensemble composed of five homogeneous absolute threshold scenarios ($\tau_i k_i = \theta$ where $\theta \in \{2, 3, 4, 5, 6\}$). As the uncalibrated CC assumes no knowledge of the estimated thresholds, and it averages the CC over a range of arbitrarily-selected threshold values, we classify it as a structure-based policy in the main text.

We implemented our own function to generate synthetic choice data and estimate the thresholds from the simulated data (see Supplementary Note S3; we implemented the two types of CC-based policies by simply passing the corresponding threshold vectors into the original function from the code by Guilbeault and Centola [41]).

S5. ADDITIONAL RESULTS FOR SEEDING POLICIES

A. Results for the ratio-to-best metric

We show here the results for the ratio-to-best metric. Specifically, to assess the relative performance of the examined seeding policies, for each analyzed configuration \mathcal{C} , we measure the simulated performance P of the nine policies. For each configuration \mathcal{C} , each method m is assigned to a performance variable that quantifies the method's performance compared to the best-performing method [64], $s_m(\mathcal{C}) = P_m(\mathcal{C}) / \max_{m'}\{P_{m'}(\mathcal{C})\}$. We average this variable across all configurations. The results, shown in Fig. S5, are largely consistent with those shown in Fig. 2 of main text.

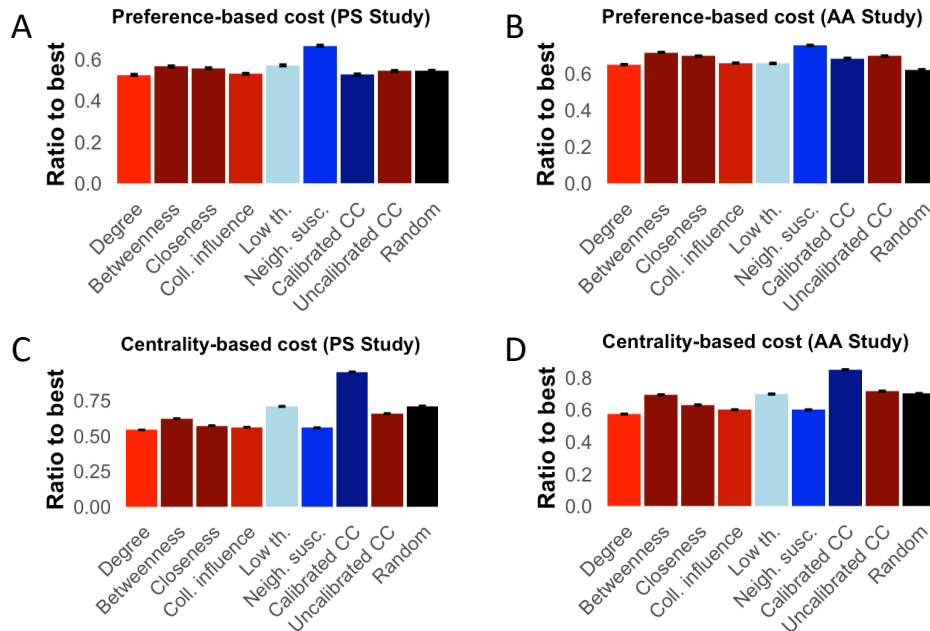


Fig. S5: **Relative performance of seeding policies according to the ratio-to-best metric.** (A, B) Relative performance of seeding policies under a preference-based cost structure, measured through the ratio-to-best metric defined above, for the policy support experiment and the app adoption experiment, respectively. The neighborhood susceptibility policy based on the estimated thresholds significantly outperforms the other policies. (C, D) Relative performance of seeding policies under a centrality-based cost structure for the policy support experiment and the app adoption experiment, respectively. The complex centrality policy based on the estimated thresholds significantly outperforms the other policies. Overall the results are in qualitative agreement with those obtained for the mean rank metric (Fig. 2 in the main text).

B. Results for different seed set sizes

We show here the results for different seed set sizes. Compared to the seed set size used in main text ($z = 0.025$), we consider here both a smaller seed set size ($z = 0.0125$) and a larger one ($z = 0.05$). The results for the smaller seed set size are in qualitative agreement with those in the main text (see Figs. S6–S7). The results for the larger seed set size are in qualitative agreement with those in the main text (see Figs. S8–S9), except for the relative performance of the methods in the preference-based cost scenario. In this scenario, the calibrated complex centrality is the best performing metric, and not the neighborhood susceptibility. The reason is arguably that with only one focal seed node selected by the neighborhood susceptibility metric, there is no guarantee that the additional seeds around the focal node require low cost. This limitation might be attenuated by network homophily, which we will investigate in a follow-up article. On the other hand, the calibrated complex centrality benefits from maximizing spreading size by taking into account clustered seeding in its calculation.

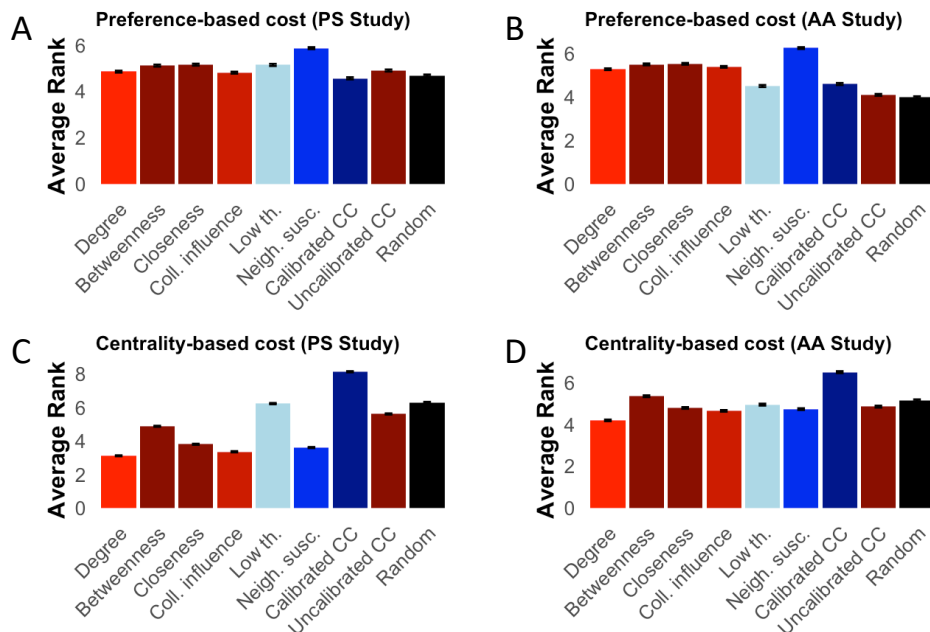


Fig. S6: **Relative performance of seeding policies for a smaller seed set size ($z = 0.0125$), according to the mean rank metric.** (A, B) Relative performance of seeding policies under a preference-based cost structure, measured through the mean rank metric used in main text, for the policy support experiment and the app adoption experiment, respectively. The neighborhood susceptibility policy based on the estimated thresholds significantly outperforms the other policies. (C, D) Relative performance of seeding policies under a centrality-based cost structure for the policy support experiment and the app adoption experiment, respectively. The complex centrality policy based on the estimated thresholds significantly outperforms the other policies. Overall the results are in qualitative agreement with those obtained with $z = 0.025$ (Fig. 2 in the main text)

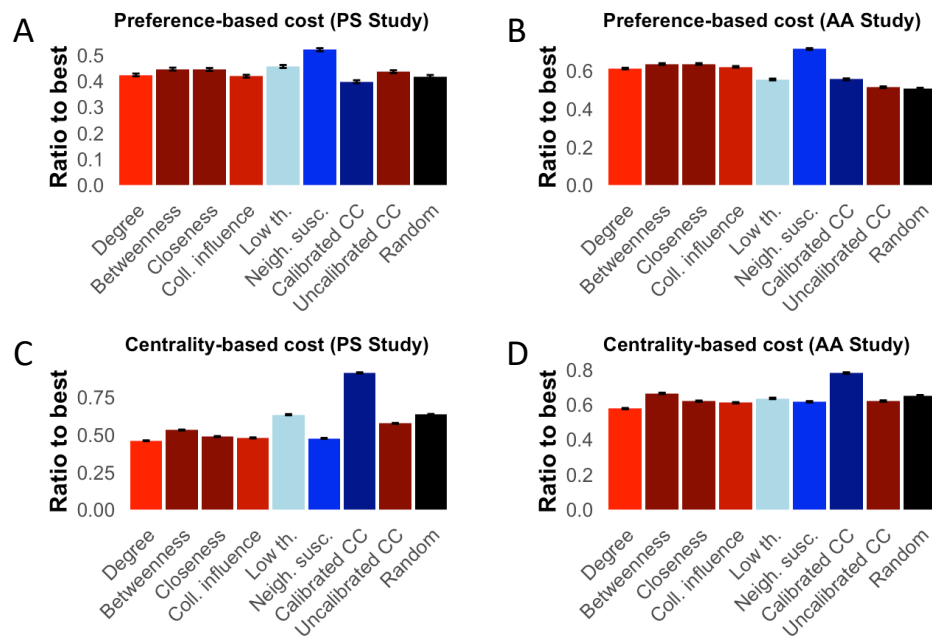


Fig. S7: Relative performance of seeding policies for a smaller seed set size ($z = 0.0125$), according to the ratio-to-best metric. (A, B) Relative performance of seeding policies under a preference-based cost structure, measured through the ratio-to-best metric defined above, for the policy support experiment and the app adoption experiment, respectively. The neighborhood susceptibility policy based on the estimated thresholds significantly outperforms the other policies. (C, D) Relative performance of seeding policies under a centrality-based cost structure for the policy support experiment and the app adoption experiment, respectively. The complex centrality policy based on the estimated thresholds significantly outperforms the other policies. Overall the results are in qualitative agreement with those obtained with $z = 0.025$ (Fig. 2 in main the text)

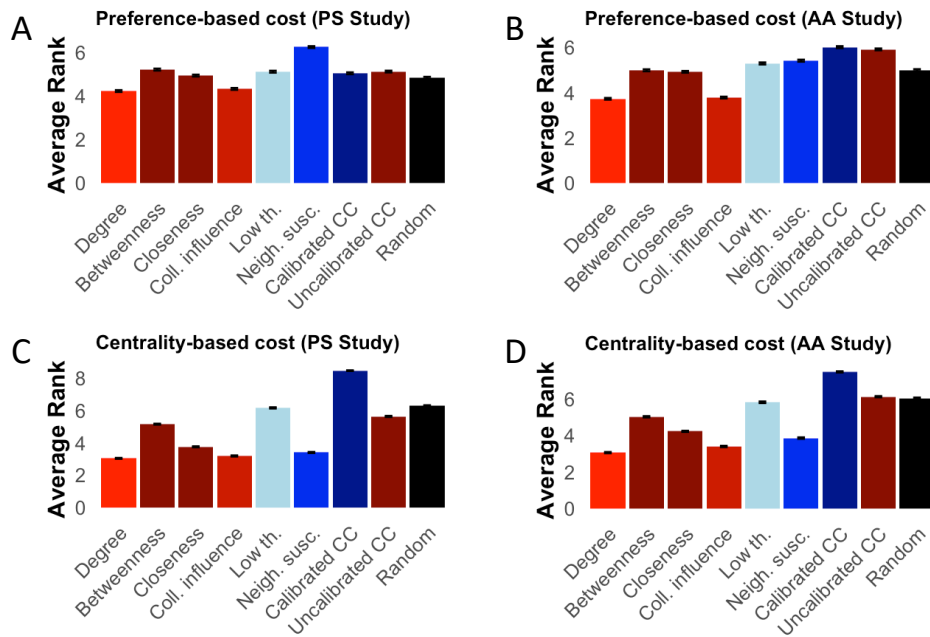


Fig. S8: **Relative performance of seeding policies for a larger seed set size ($z = 0.05$), according to the mean rank metric.** (A, B) Relative performance of seeding policies under a preference-based cost structure, measured through the mean rank metric used in main text, for the policy support experiment and the app adoption experiment, respectively. In the simulations calibrated with the AA study results, the neighborhood susceptibility policy is not anymore the best-performing metric: For a larger seed set, the threshold information encoded in a node's nearest neighborhood is not anymore sufficient to identify an effective focal seed. (C, D) Relative performance of seeding policies under a centrality-based cost structure for the policy support experiment and the app adoption experiment, respectively. The complex centrality policy based on the estimated thresholds significantly outperforms the other policies. Overall the results are in qualitative agreement with those obtained with $z = 0.025$ (Fig. 2 in the main text).

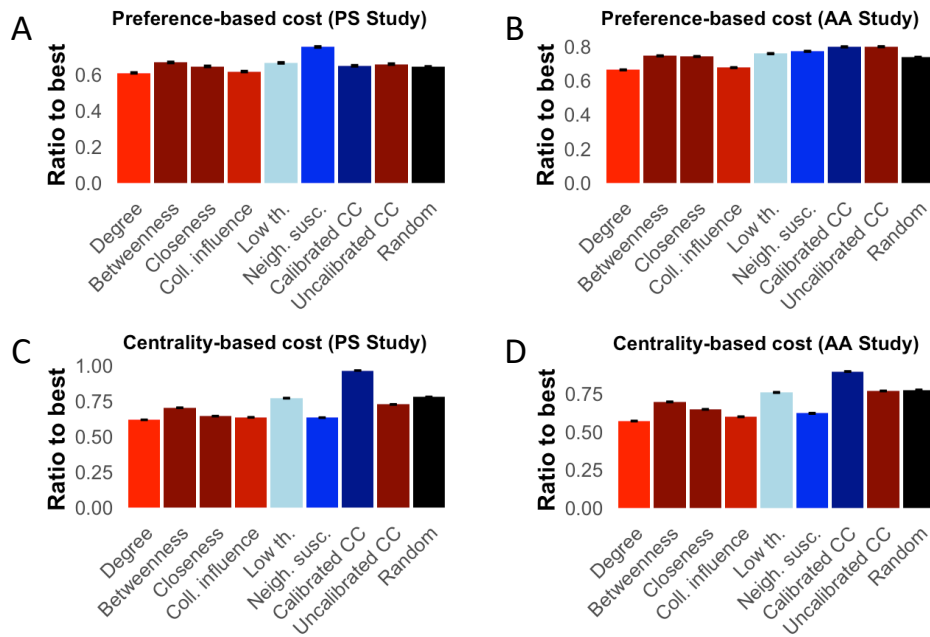


Fig. S9: **Relative performance of seeding policies for a larger seed set size ($z = 0.05$), according to the ratio-to-best metric.** (A, B) Relative performance of seeding policies under a preference-based cost structure, measured through the ratio-to-best metric defined above, for the policy support experiment and the app adoption experiment, respectively. Again, in the simulations calibrated with the AA study results, the neighborhood susceptibility policy is not anymore the best-performing policy. (C, D) Relative performance of seeding policies under a centrality-based cost structure for the policy support experiment and the app adoption experiment, respectively. The complex centrality policy based on the estimated thresholds significantly outperforms the other policies.

C. Results in scenarios with partial threshold data

We consider scenarios where the social change practitioner has been only able to survey a fraction ρ of the network's nodes. In this scenario, we assume that the low-threshold and neighborhood-susceptibility policies only consider as candidate focal seed nodes those nodes that have been surveyed. For simplicity, we do not consider the calibrated complex centrality here, and narrow our focus to the preference-based cost scenario.

As anticipated in the main text, we find that for both experiments, the relative advantage of the neighborhood susceptibility policy is robust with respect to incomplete data as far as more than the large majority of the nodes is surveyed (e.g., 75%, see Figs. S10-S14). At the same time, it remains robust with respect to highly incomplete data (e.g., 50% or fewer surveyed nodes) only in the PS experiment, but not in the AA experiment. This is arguably due to the larger number of low-threshold nodes in the PS experiment, which makes the identification of low-threshold nodes simpler even with highly incomplete data. We note that in order to save computational time, for the simulations carried out in this Section, we only used one realization of the simulated conjoint survey performed by the change practitioner to estimate the thresholds (as opposed to five in all other Sections, see Supplementary Note S3).

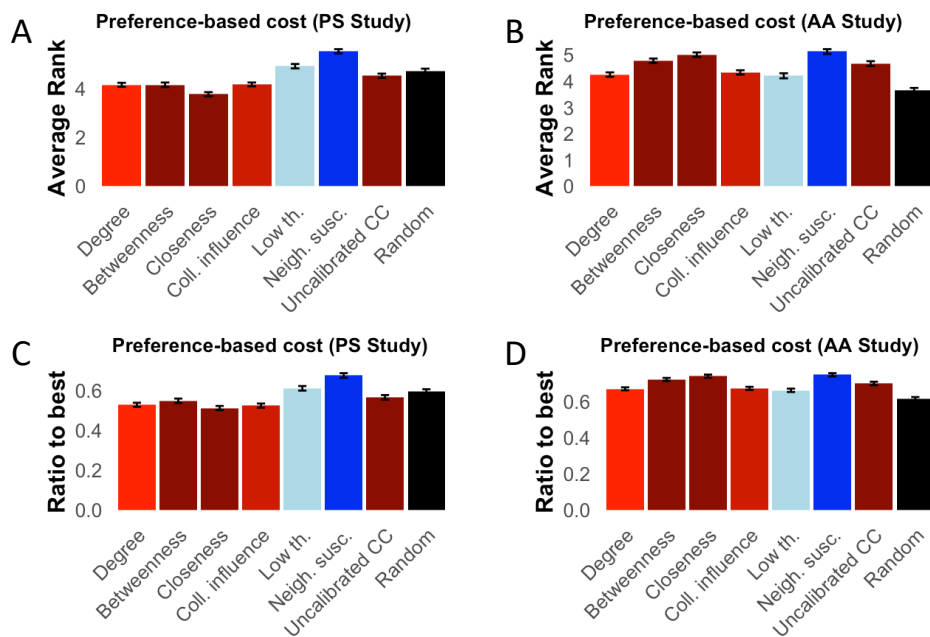


Fig. S10: **Relative performance of seeding policies when 90% of the nodes are surveyed.** Relative performance of seeding policies under a preference-based cost structure, measured through the mean rank metric used in main text (A, B) and through the ratio-to-best metric defined above (C, D) for the policy support experiment and the app adoption experiment, respectively. The neighborhood susceptibility policy based on the estimated thresholds outperforms the other policies, although its edge over the closeness policy is slim in the simulations calibrated with the AA study.

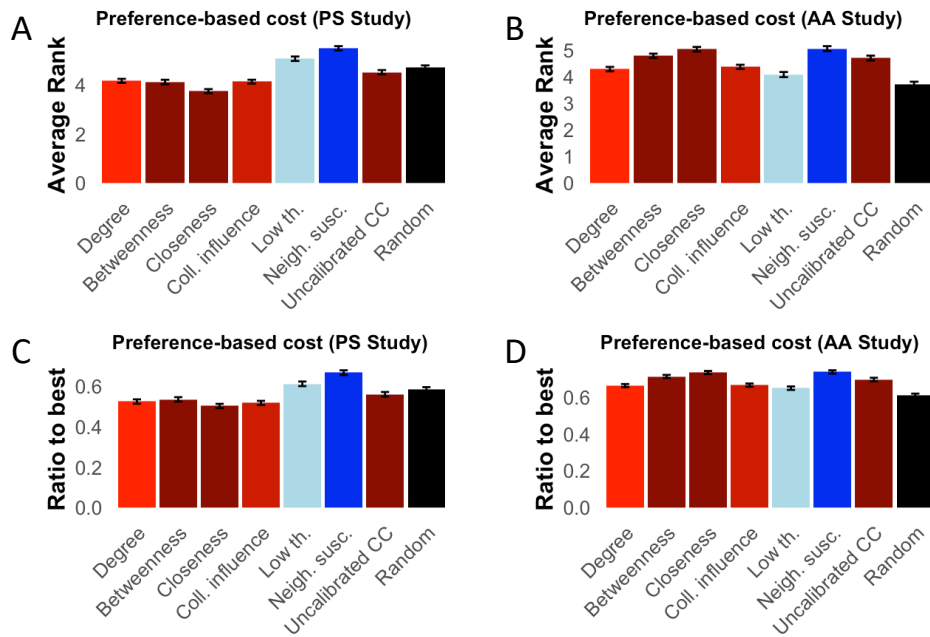


Fig. S11: **Relative performance of seeding policies when 75% of the nodes are surveyed.** Relative performance of seeding policies under a preference-based cost structure, measured through the mean rank metric used in main text (A, B) and through the ratio-to-best metric defined above (C, D) for the policy support experiment and the app adoption experiment, respectively. The neighborhood susceptibility policy based on the estimated thresholds outperforms the other policies, although its edge over the closeness policy is slim in the simulations calibrated with the AA study.

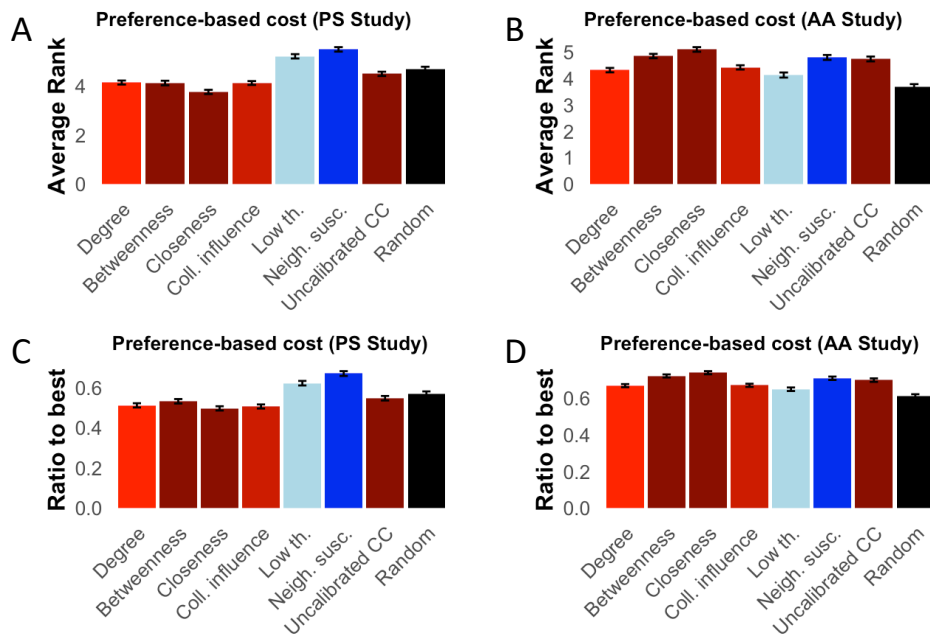


Fig. S12: **Relative performance of seeding policies when 50% of the nodes are surveyed.** Relative performance of seeding policies under a preference-based cost structure, measured through the mean rank metric used in main text (A, B) and through the ratio-to-best metric defined above (C, D) for the policy support experiment and the app adoption experiment, respectively. In the simulations calibrated with the AA experiment, the neighborhood susceptibility policy based on the estimated thresholds does not outperforms the others anymore.

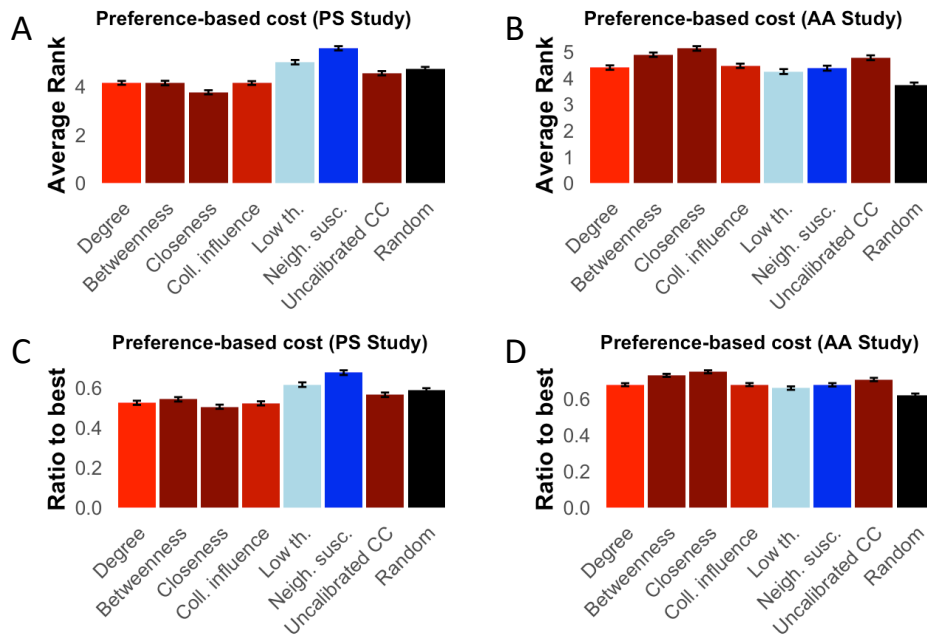


Fig. S13: **Relative performance of seeding policies when 25% of the nodes are surveyed.** Relative performance of seeding policies under a preference-based cost structure, measured through the mean rank metric used in main text (A, B) and through the ratio-to-best metric defined above (C, D) for the policy support experiment and the app adoption experiment, respectively. In the simulations calibrated with the AA experiment, the neighborhood susceptibility policy based on the estimated thresholds does not outperforms the others anymore.

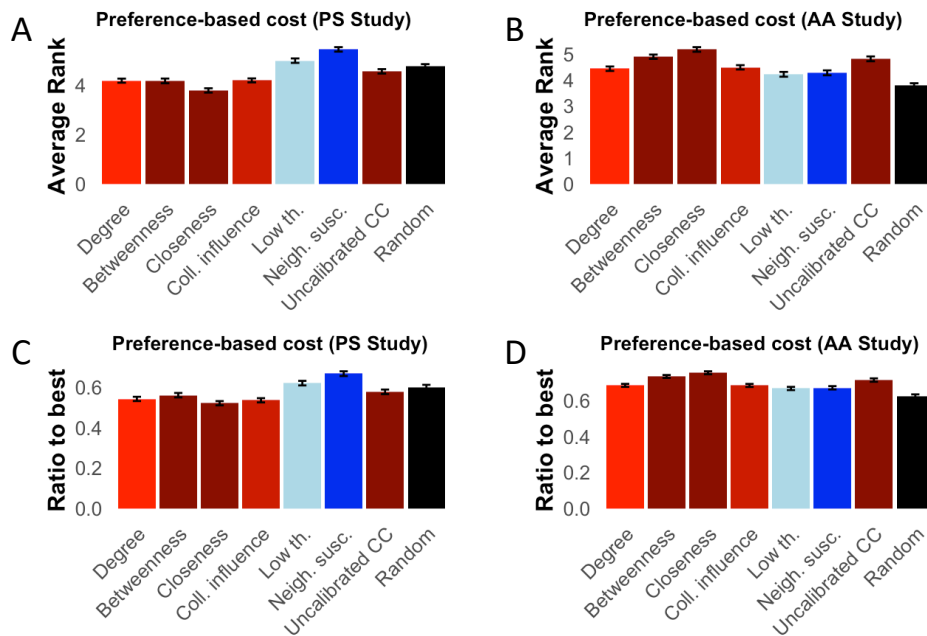


Fig. S14: **Relative performance of seeding policies when 10% of the nodes are surveyed.** Relative performance of seeding policies under a preference-based cost structure, measured through the mean rank metric used in main text (A, B) and through the ratio-to-best metric defined above (C, D) for the policy support experiment and the app adoption experiment, respectively. In the simulations calibrated with the AA experiment, the neighborhood susceptibility policy based on the estimated thresholds does not outperforms the others anymore.

S6. LINKING INDIVIDUAL-LEVEL CHOICE MODELS WITH SOCIAL SPREADING THEORIES

A. Linking individual utilities and adoption probabilities

In general terms, discrete choice theory [3] considers behavioral models $y = h(x, \epsilon)$ that describes how an individual-level choice y is determined by some observable properties x and some unobservable ones, ϵ , where ϵ follows a certain distribution, $\epsilon \sim f(\epsilon)$. The goal is typically to obtain the probability that an individual makes choice y , $\Pi(y|x)$, given the observable properties x . The theory assumes that an individual n chooses among I alternatives $i \in \{1, \dots, I\}$ in such a way to maximize her utility

$$U_{ni} = U_{ni}^* + \epsilon_{ni}, \quad (6)$$

where U_{ni}^* depends on observable properties of individual n and alternative i , whereas ϵ_{ni} is an error term drawn from a certain distribution f : $\epsilon_{ni} \sim f(\epsilon_{ni})$. One can show that if $\epsilon_{i\alpha}$ s are i.i.d. variables extracted from an extreme value distribution (Gumbel, $f(\epsilon) = \exp(-\epsilon) \exp(-\exp(-\epsilon))$), then the probability that individual n chooses alternative i is simply [3]

$$\Pi_{ni} = \frac{\exp(U_{ni}^*)}{\sum_{j=1}^I \exp(U_{nj}^*)}. \quad (7)$$

Eq. (7) can be also derived via statistical physics methods, by assuming that an individual maximizes her expected utility plus the variety of her available options, represented by the entropy of the choice probability distribution [93]. For a *binary choice* between not adopting and adopting a given product i , we simplify the notation and denote by Π_{ni} and $\bar{\Pi}_{ni} = 1 - \Pi_{ni}$ the probabilities that n adopts and does not adopt product i , respectively. We have:

$$\Pi_{ni} = \frac{1}{1 + \exp(\bar{U}_{ni}^* - U_{ni}^*)}, \quad (8)$$

where we denoted with U_{ni}^* and \bar{U}_{ni}^* the systematic utilities from adopting and not adopting, respectively. In the following, we shall use these results to derive collective adoption models. It is useful to consider a clarity parameter [94] and, with a slight abuse of notation, rewrite the utility from alternative i in the form

$$U_{ni} = cU_{ni}^* + \epsilon_{ni}. \quad (9)$$

The clarity parameter rules the relative importance of the systematic and stochastic components; in the statistical physics language, it can be referred to as inverse temperature [93]. We can consider two regimes: high clarity ($c \gg 1$) and low clarity ($c \ll 1$). In the binary case, in the high-clarity regime,

$$\Pi_{ni} = \frac{1}{1 + \exp(c(\bar{U}_{ni}^* - U_{ni}^*))} \simeq \Theta(U_{ni}^* - \bar{U}_{ni}^*), \quad (10)$$

where Θ is the Heaviside function. This represents a threshold rule [94], which will be useful in the following. In the low-clarity regime, we use the property that $(1 + \exp \epsilon)^{-1} \simeq 1/2 - \epsilon/4$. Therefore,

$$\Pi_{ni} \simeq \frac{1}{2} + \frac{c}{4}(U_{ni}^* - \bar{U}_{ni}^*) + \mathcal{O}(c^2). \quad (11)$$

The threshold-like probability obtained in the high-clarity regime and the linear probability obtained in the low-clarity regime can be linked to the adoption probabilities for a complex and a simple social contagion model, respectively, as shown below.

B. Complex contagion theory

Consider a scenario where an individual makes a binary choice about whether to adopt product i . As in the main text, suppose that the systematic component of her utility from adopting product i is:

$$\bar{U}_{ni}^* = c \left(\sum_a \beta_{na} x_{ia} + \gamma_n s_{ni} \right) = c(U_{ni}^{(A)} + \gamma_n s_{ni}). \quad (12)$$

Suppose that the utility from not adopting is fixed, $\bar{U}_n^* = U_n^{(0)}$, where $U_n^{(0)}$ could represent the price, the risk from adopting, or some product-specific cost of adopting. From Eq. (10), it follows that

$$\Pi_{ni} = \frac{1}{1 + \exp(c(U_n^{(0)} - U_{ni}^{(A)} - \gamma_n s_{ni}))}. \quad (13)$$

For $U_{ni}^{(A)} = 0$, only social signals affect individuals' adoption decisions, and we recover the logistic model referred to as burden of social proof model [94]. In the limit of large c (high clarity), $\Pi_{ni} = 1$ if and only if

$$U_n^{(0)} - U_{ni}^{(A)} - \gamma_n s_{ni} > 0, \quad (14)$$

which can be rewritten as

$$s_{ni} > \gamma_n^{-1}(U_n^{(0)} - U_{ni}^{(A)}) = \tau_{ni}, \quad (15)$$

from which Eq 1 in the main text follows. This condition shows that the threshold model can be derived from the individual-level choice mechanism, and the threshold can be interpreted in terms of individual-level and product-level attributes [47]. Note that the proposed interpretation of the threshold enables a reinterpretation of the innovators and early adopters, widely-studied adopter types in the innovation diffusion literature [48]. In Eq. (15), attribute utility values such that $U_{ni}^{(A)} \geq U_n^{(0)}$ lead to $\tau_{ni} \leq 0$, which means that the individual is willing to adopt as soon as she is informed about the new product, thereby behaving as natural innovators.

The proposed interpretation of the threshold model also enables a natural interpretation of the cost or effort needed to persuade an individual to adopt a new product in the absence of social signal, which is the case at the seeding stage, when the diffusion has not started yet. In this case, $U^{(S)} = 0$; one can interpret the cost of targeting as the utility increase needed such that $U_{ni} > \bar{U}_{ni}$ is verified. We add the effort term, $U_{ni}^{(E)}$, to the utility as

$$U_{ni}^*(t) = U_{ni}^{(A)} + U_{ni}^{(E)}. \quad (16)$$

Although efforts to incentivize adoption can take various forms [95], to fix ideas, we interpret $U_{ni}^{(E)}$ as the result of a monetary incentive offered by the practitioner to individual n in order to persuade her to adopt i . For simplicity, we assume $U_{ni}^{(E)} = \mu_n (c_{ni} - c_0)$, where c_{ni} denotes the cost of targeting n individual to promote i , c_0 denotes a fixed acquisition cost [67], and μ_n denotes n 's sensitivity to the targeting offer. Under these assumption, in the beginning of the diffusion, n adopts only if $U_{ni}^{(A)} + U_{ni}^{(E)} \geq U_n^{(0)}$; the minimal incentive for this condition to hold is

$$\kappa_{ni} = c_0 + \mu_n^{-1}(U_n^{(0)} - U_{ni}^{(A)}). \quad (17)$$

This result is intuitive: the cost to effectively target n for product i is higher the higher the resistance ($R_{ni} = U_n^{(0)} - U_{ni}^{(A)}$) between her status-quo utility and her attribute utility. It aligns with the literature on social norms, which posits that successfully targeting initially-resistant agents requires higher incentive [1, 16, 96]. In main text, we set $c_0 = 0, \mu_n = 1$; in this case, Eq. (17) outputs negative values of κ_{ni} for individuals with $R_{ni} < 0$; we assume that the effective cost of successfully targeting these individuals is zero. In main text, we also consider a scenario where the cost of targeting depends on the centrality of the prospect target, which better aligns with the literature on influencers in social media [65, 68].

C. Simple contagion: Bass model

The Bass model assumes that faced with the binary choice of whether to adopt a new product or not, the probability that individual n adopts at a given time t is $\Pi_n(t) = p_n + q_n s_n(t)$, where $s_n(t)$ is the social signal received by n at time t about the product, and p, q denote the innovation and innovation coefficient, respectively; for simplicity in this section, we omit the product subscript (i) from the notation. In a fully-connected network, $s_n(t) = s(t)$ denotes n 's cumulative number of adopters at time t , which in a homogeneous preference scenario ($p_n = p, q_n = q$), leads to the original formulation of the Bass model [42]. When the potential adopters are embedded in a non-trivial network topology, $s_n(t)$ can represent the fraction of n 's social contacts who already adopted the product [69]. Following Centola and Macy's terminology [22], the Bass model can be interpreted as a *simple contagion model* as individuals have a non-zero probability of adopting even if only one of their social contacts already adopted (even when $p = 0$).

We show that the Bass model can be reinterpreted in terms of individual-level utility functions. Similarly as above, we assume that individual n 's utility from adopting the new product at a given time t is $U_n^*(t) = U_n^{(A)} + \gamma_n s_n(t)$,

where $U_n^{(A)}$ could be expressed, as in the main text, as a linear combination of the product attributes; again, γ_n denotes the marginal utility of social signals for n . We assume again that the status-quo utility from not adopting is fixed: $\bar{U}_n^*(t) = U_n^{(0)}$, where $U_n^{(0)}$ is a parameter that could represent the price or risk associated with the adoption. In the low-clarity regime Eq. (11), we obtain that Π_n follows the Bass equation with innovation parameter $p_n = (1 - c(U_n^{(0)} - U_n^{(A)}))/2 = 1/2 - cR_n/4 = 1/2 - R_n/T$ and imitation parameter $q_n = c\gamma_n/4 = \gamma_n/T$, where we defined the temperature parameter [11, 93] as $T = 4/c$, where factor 4 is introduced solely for cosmetic reasons. The role of temperature parameter T influences the Bass model's parameter: In the infinite-temperature limit, the choice is only determined by the stochastic component of the utility. In this limit, the innovation parameter reflects a coin flip (1/2 probability) and the social signal plays no role (zero imitation parameter). As the temperature is large (necessary to derive the linear adoption probability) but finite, p_n deviates from 1/2 and $q_n > 0$. The finite-temperature result matches our intuition: the higher the resistance of individual n for the product, the lower the innovation coefficient; the higher n 's marginal utility from the social signal, the higher the imitation coefficient.

This simple argument shows that not only complex contagion models, but also simple contagion ones can be reinterpreted in terms of the proposed micro-level framework. Under standard assumption in discrete-choice theory, if the utility from adopting grows as a power-law of the social signal, the two considered complex and simple contagion models emerge naturally in the high- and low-clarity regimes. Taken together, these findings suggest that individual-level models might benefit policies to maximize or prevent social spreading for a broader class of models than the complex contagion one studied in the main text. We leave the derivation of alternative models of simple contagions (e.g., rumor spreading models [97] and empirical diffusion models [17]) for future research.

D. Preferential attachment and fitness models

Pure preferential attachment. When applied to social systems, preferential attachment models capture the collective recognition received by cultural products such as scientific papers [43], patents [98], books [99], and online articles [100] as well as individuals in collaboration networks [101], among others. We assume that individual n is faced with I alternatives, and that her utility from adopting is affected by the aggregate social signal, s , she receives about each of the alternatives, which represents their total number of previous adopters. Assume that individual n exhibits decreasing marginal utility from the social signal, which means that in response to an increase ds in the social signal received about a given product, her utility for that alternative increases by $du = \gamma ds/s$. Under this assumption, the systematic component of n 's utility from adopting i is

$$U_{ni}^* = \gamma_n \log(s_i). \quad (18)$$

Under this assumption, whenever n makes a new adoption decision among $I(t)$ available alternatives at time t , from Eq. (7), the probability she chooses i is

$$P_{ni} = \frac{s_i^{\gamma_n}}{\sum_{j=1}^{I(t)} s_j^{\gamma_n}}, \quad (19)$$

where the sum in the denominator runs over the $I(t)$ available alternatives at time t . Eq. (19) corresponds to a nonlinear preferential attachment model with heterogeneous exponent. If $\gamma_n = \gamma$ is homogeneous, we recover a standard nonlinear preferential attachment model [70]; with $\gamma = 1$, we recover the standard preferential attachment model, as noted by ref. [77] in the context of network formation models. It is interesting to note how a mild preference for more popular alternatives can be amplified when moving from the individual-level utility function to the collective adoption dynamics: The utility function scales only logarithmically with s (Eq. (18)), but the probability of adoption scales linearly with s (Eq. (19)); in the collective dynamics, this results in extreme success inequalities (heavy-tailed distribution of s [70]).

Generalized preferential attachment and fitness models. Preferential attachment is not the only driving factor in state-of-the-art models for characterizing and predicting the dynamics of scientific impact [43, 73], book sales [99]. These studies consider more sophisticated models where alternatives are characterized by their fitness level (which captures the intrinsic attractiveness of an alternative's qualities to the potential adopters) and an aging function (which can capture the lower attractiveness of older alternatives or more complex temporal patterns, e.g., for scientific paper impact [43, 73]). To derive the relevance model [73], consider the following utility from adopting alternative i :

$$U_{ni}^*(t) = \gamma_n \log(s_i(t)) + U_{ni}^A + \delta_n \phi(t - t_i), \quad (20)$$

where:

- The first preferential attachment term is analogous to Eq. (18).
- The “fitness” component of the utility, U_{ni}^A , is analogous to the attribute utility in main text. As in main text, in line with the consumer behavior literature, it could be operationalized as $U_{ni}^A = \sum_a \beta_{na} x_{ai}$, where x_{ai} is the value taken by attribute a for alternative i and β_{na} captures n ’s preference for attribute a .
- The age-dependent component of the utility depends on function $\phi(t - t_i)$ depends on alternative i ’s age (where t_i denotes the time at which i enters the system), while δ_n denotes n ’s preference for old products, which could vary across individuals [57, 102].

With this utility function, the probability that n adopts α at time t is

$$\Pi_{ni}(t) = \frac{s_i(t)^{\gamma_n} \exp(U_{ni}^A) \exp(\delta_n \phi(t - t_i))}{\sum_j s_j(t)^{\gamma_n} \exp(U_{nj}^A) \exp(\delta_n \phi(t - t_j))} \quad (21)$$

where $\exp(U_{ni}^A)$ captures the intrinsic attractiveness of i ’s attributes for individual n and $\Phi(t - t_i) = \exp(\phi(t - t_i))$ plays the role of an aging function (note that a linear preference for more recent items in the utility function results in an exponential aging function). With suitable simplifying assumptions, we can recover various preferential attachment models from this expression.

- *Preferential attachment with fitness and aging.* When $\gamma_n = 1$ (homogeneous susceptibility to the social signal), $\delta_n = 1$ (homogeneous age preference), $\beta_{na} = \beta_a$ (homogeneous attribute preference), we obtain the preferential attachment with fitness and aging [43]:

$$\Pi_{ni}(t) = \Pi_i(t) = \frac{s_i(t) \eta_i \Phi(t - t_i)}{\sum_j s_j(t) \eta_j \Phi(t - t_j)}, \quad (22)$$

where an alternative’s fitness is provided by $\eta_i = \exp(\sum_a \beta_a x_{ai})$. A related model can be also obtained without the homogeneous preference assumption, under the mean-field assumption² that the denominator of Π_i converges toward a constant value Ω^* [73]. Under this assumption, the rate at which alternative i attracts more choices is $\propto s_i(t) \tilde{\eta}_i \Phi(t - t_i)$, where $\tilde{\eta}_i$ provides an alternative interpretation of an alternative’s fitness as the average of the individuals’ preference factor, $\exp(U_{ni}^A)$, in line with the interpretation in Refs. [43, 103].

- *Preferential attachment with fitness.* Under the homogeneous preference assumption, by setting $\delta_n = 0$, we obtain the Bianconi-Barabási model [72].
- *Fitness models without preferential attachment.* By setting $\gamma_n = 0$, fitness models without preferential attachment like those considered by Refs. [104, 105] can be obtained.
- *Preferential attachment with homophily.* Models that take into account homophily include the popularity-similarity model [74] and the more recent model in ref. [75]. For example, the preferential attachment with homophily model by ref. [75] can be simply obtained from Eq. (21) by setting $\gamma_n = 1$ and $\delta_n = 0$.
- *Heterogeneous models.* Using Eq. (21), one can derive preferential attachment models that include behavioral heterogeneity.

² See Medo et al. [73] for a detailed discussion of the plausibility

and range of applicability this approximation.